Thesis for the degree of Doctor of Philosophy

MICROFABRICATION TECHNIQUE APPLICATIONS
From Passive Particle Manipulation To Active Microswimmers, Micromachines, And Fluidic Control

Gan Wang

Department of Physics
University of Gothenburg

Göteborg, Sweden 2025

UNIVERSITY OF GOTHENBURG

Microfabrication Technique Applications From Passive Particle Manipulation To Active Microswimmers, Micromachines, And Fluidic Control

Gan Wang
978-91-8115-044-5 (printed)
978-91-8115-044-3 (electronic)

Department of Physics
Universitet of Gotheburg, SE-412 96 Göteborg
Tel: +46 (0)31-727685737
http://www.physics.gu.se

Printed by STEMA SPECIALTRYCK AB
Borås, Sweden 2025

Sammanfattning

Att begränas den Brownska rörelsen på mikro- och nanometerskalan för att uppnå precis kontroll över objekt är avgörande inom materialvetenskap och biologi. Betydande framsteg har gjorts i att fånga och manipulera mikroskopiska objekt, antingen genom att skapa gradienter via externa fysiska fält eller genom att konstruera system som utvinner energi för autonom rörelse. Dessa tekniker bygger på exakt tillämpning av optiska och elektromagnetiska krafter, och nya framsteg inom mikro- och nanofabrikation har öppnat möjligheter för effektiv manipulation av mikroskopiska objekt.

Denna avhandling tillämpar traditionella mikro- och nanofabrikationstekniker för att skapa mikro- och nanostrukturer som manipulerar krafter, främst den kritiska Casimir-kraften och optiska krafter, för att kontrollera mikroskopiska objekt. Jag visar att periodiska mikromönsterkan kan tillverkas på ett substrat och att kemisk funktionalisering kan ge hydrophila och hydrofoba egenskaper. Vid den kritiska temperaturen av en binär vätska genereras attraktiva och repulsiva Casimir-krafter mellan mönstren och mikropartiklarna, vilket möjliggör stabil infångning och manipulation av partiklarna. Man övergår därvid från passiv kontroll till aktiv rörelse genom metaytor som modulera det optiska fältet och integreras i mikropartiklar (mikrosimmare). Detta möjliggör ljus- och rörelsemängdstutbyte under laserbelysning, vilket ger en autonom rörelse. Genom att variera designen av metaytorna och ljusets intensitet och polarisation kan komplexa beteenden uppstå hos dessa mikrosimmare. Därefter integreras mikrosimmarna på ett chip, vilket skapar "on-chip"-mikromotorer kopplade via växelkonstruktioner, som bildar miniatyrmaskiner som kan utföra olika funktionella uppgifter. Genom att ändra konfigurationen och avstånden mellan maskinerna kan precis, multifunktionell kontroll över fluiddynamik uppnås, vilket underlättar transport av mikroskopiska objekt. Resultaten från denna forskning indikerar innovativa metoder för skalbar och effektiv manipulation av partiklar, mer intelligenta mikrorobotar och kraftfulla miniatyriserade "on-chip"-maskiner, med tillämpningar inom en rad olika områden och branscher.

Keywords:mikro- och nanoskalig manipulation, mikro- och nanofabrikation, kritisk Casimir-kraft, mikrosimmare, metasurface, mikromaskin, fluidkontroll

Abstract

Overcoming Brownian motion at the micro- and nanoscale to achieve precise control of objects is crucial for fields such as materials science and biology. Significant progress has been made in trapping and manipulating micro- and nanoscale objects, either by generating gradients through external physical fields or by engineering systems that can harvest energy from their environment for autonomous motion. These techniques rely on the precise application of forces, such as optical and electromagnetic forces, and have found extensive applications across various scientific disciplines. Recent advances in micro- and nanofabrication technologies have greatly enhanced the generation and regulation of these forces, offering new possibilities for manipulating micro- and nanoscale objects.

This thesis applies traditional micro- and nanofabrication techniques, typically used in semiconductor manufacturing, to construct micro- and nanostructures for manipulating forces, primarily critical Casimir forces and optical forces, to achieve precise control over microscale object movement.

I first show the fabrication of periodic micropatterns on a substrate, followed by chemical functionalization to impart hydrophilic and hydrophobic properties. Near the critical temperature of a binary liquid, attractive and repulsive critical Casimir forces are generated between the micropatterns and microparticles. These forces allow the stable trapping of the microparticles on the substrate and the manipulation of their configuration and movement. Then, my research transitions from passive control to active motion by fabricating metasurfaces capable of modulating optical fields and embedding them within micro-particles (microswimmers). This enables light-momentum exchange under planar laser illumination, resulting in autonomous movement of the microswimmers. By varying the metasurface design as well as the intensity and polarization of the light, complex behaviors can emerge within these microswimmers. Subsequently, My research focused on using these microfabrication techniques to build micromotors integrated on a chip surface. These micromotors couple with other objects through gear structures, creating miniature machines that can execute functional tasks. Finally, by altering the configuration of these machines and the distances between them, I acheived precise, multifunctional control over fluid dynamics, facilitating the transport of micro- and nanoscale objects.

Insights gained from this research suggest innovative manufacturing approaches for scalable manipulation of particles, more intelligent microrobots, and powerful miniaturized on-chip machines, with applications across various fields.

Keywords: micro- and nanoscale manipulation, micro-nano fabrication, microswimmer, critical Casimir force, metasurface. micromachine, fluid control

This thesis is based on the work contained in the following scientific papers.

- **Paper I: Nanoalignment by critical Casimir torques**
  Gan Wang, Piotr Nowakowski, Nima Farahmand Bafi, Benjamin Midtvedt, Falko Schmidt, Agnese Callegari, Ruggero Verre, Mikael Käll, S Dietrich, Svyatoslav Kondrat, Giovanni Volpe
  Nature Communication **15**, 5086, (2024).

- **Paper II: Light-Driven Microengines with Complex Behavior**
  Preliminary list of authors in alphabetical order: Agnese Callegari, Mikael Käll, Edoardo Manoni, Mahdi Shanei, Giovanni Volpe, **Gan Wang**
  Manuscript in preparation.

- **Paper III: Microscopic Geared Mechanisms**
  Gan Wang, Marcel Rey, Antonio Ciarlo, Mahdi Shanei, Kunli Xiong, Giuseppe Pesce, Mikael Käll, Giovanni Volpe
  arXiv preprint arXiv:2409.17284 (2024).

- **Paper IV: On-Chip Light-Driven Micromotors for Microfluidic Manipulation**
  Preliminary list of authors in alphabetical order: Antonio Ciarlo, Mikael Käll, Adrian Paskert, Giuseppe Pesce, Marcel Rey, Mahdi Shanei, Giovanni Volpe, **Gan Wang**, Raphael Wittkowski, Kunli Xiong
  Manuscript in preparation.

Additional publications that are not included in the context of this thesis.

- **Paper V: Transverse optical gradient force in untethered rotating metaspinners**
  Einstom Engay, Mahdi Shanei, Vasilii Mylnikov, **Gan Wang**, Peter Johansson, Giovanni Volpe, Mikael Käll
  arXiv preprint arXiv:2406.11489, (2024).

- **Paper VI: Video-Rate Switching of High-Reflectivity Hybrid Cavities Spanning All Primary Colors**
  Kunli Xiong, Oliver Olsson, Stefano Rossi, **Gan Wang**, Magnus P Jonsson, Andreas Dahlin, Jeremy J Baumberg
  Advance Materials. **35**, 2302028, (2023).

- **Paper VII: Quantitative studies of single-molecule chemistry using conductance measurement**
  Biao-Feng Zeng, Yu-Ling Zou, **Gan Wang**, Wenjing Hong, Zhong-Qun Tian, Yang Yang
  Nano Today. **47**, 101660, (2022).

- **Paper VIII: In situ lattice tuning of quasi-single-crystal surfaces for continuous electrochemical modulation**
  Biao-Feng Zeng, Jun-Ying Wei, Xia-Guang Zhang, Qing-Man Liang, Shu Hu, **Gan Wang**, Zhi-Chao Lei, Shi-Qiang Zhao, He-Wei Zhang, Jia Shi, Wenjing Hong, Zhong-Qun Tian, Yang Yang
  Chemical Science. **13**, 7765, (2022).

- **Paper IX: Selective Fabrication of Single-Molecule Junctions by Interface Engineering**
  Biao-Feng Zeng, **Gan Wang**, Qiao-Zan Qian, Zhi-Xin Chen, Xia-Guang Zhang, Zhi-Xing Lu, Shi-Qiang Zhao, An-Ni Feng, Jia Shi, Yang Yang, Wenjing Hong
  Small. **16**, 2004720, (2022).

- **Paper X: Single-molecule plasmonic optical trapping**
  Gan Wang, Chao Zhan, Jun Yi, Jun-Ying Wei, Zhi-Hao Li, Zhao-Bin Chen, Jia Shi, Yang Yang, Wenjing Hong, Zhong-Qun Tian
  Matter. **3**, 1350, (2020).

- **Paper XI: Automatic classification of single-molecule charge transport data with an unsupervised machine-learning algorithm**
  Feifei Huang, Ruihao Li, **Gan Wang**, Jueting Zheng, Yongxiang Tang, Junyang Liu, Yang Yang, Yuan Yao, Jia Shi, Wenjing Hong
  Physical Chemistry Chemical Physics. **22**, 1674, (2020).

- **Paper XII: Single-Molecule Measurement of Adsorption Free Energy at the Solid–Liquid Interface**
  Gan Wang, Chao Zhan, Xia-Guang Zhang, Zhi-Hao Li, Jun-Ying Wei, Yu Si, Yang Yang, Wenjing Hong, Zhong-Qun Tian
  Angewandte Chemie International Edition. **58**, 14534, (2019).

- **Paper XIII: Application of electrochemistry to single-molecule junctions: from construction to modulation**
  Gan Wang, Biao-Feng Zeng, Shi-Qiang Zhao, Qiao-Zan Qian, Wenjing Hong, Yang Yang
  Science China Chemistry **62**, 1333, (2019).

Contents

Chapter 1

Introduction

Since my undergraduate studies, I have been thinking about the relationship between science and technology, especially how they complement and integrate with each other. Science seeks to discover the basic laws of Nature, while technology focuses on applying these theories to real-world problems. As I moved forward in my doctoral research, I realized that there are no clear boundaries between them; rather, they are interconnected and advance together. A notable example is laser technology. The theoretical basis for lasers comes from Einstein's 1917 theory of stimulated emission [1], a fundamental discovery in quantum mechanics. Scientists studied photon behavior to understand how to control and amplify light, establishing the scientific foundation for the laser. By the 1960s, technological advances enabled the practical realization of this theory, exemplified by Theodore Maiman's creation of the first laser [2]. The impact of lasers extends beyond their initial invention, as they drive further scientific research, such as precision measurement [3] and laser cooling of atoms [4], particles trapping experiments [5]. Part of the research conducted in this thesis builds on this foundation by utilizing lasers to control the movement of microparticles. This exemplifies how science and technology support each other, fostering progress and new discoveries in the modern world.

This synergy between science and technology is mirrored in another significant trend observed over the past fifty years: the advancements driven by Moore's Law, which predicts that the number of transistors on integrated circuits will double approximately every 18 to 24 months [6]. This trend has been crucial to the global technological revolution, reflecting how theoretical insights in semiconductor physics have informed practical innovations. As transistor sizes have continued to shrink to just a few nanometers and shifted toward three-dimensional integration [7], computer performance has dramatically increased, resulting in devices that are more compact and energy-efficient. These advancements have enabled the realization of transformative technologies such as personal computers, smartphones, Internet of Things (IoT) devices, and artificial intelligence (AI).

Moreover, Moore's Law has not only advanced the development of electronic devices but has also propelled progress in micro- and nanofabrication technologies. Photolithography has evolved from mercury lamp sources with wavelengths of 436 nm (g line) and 365 nm (I line) to deep ultraviolet (DUV) sources at 248 nm (KrF) and 193 nm (ArF), and ultimately to extreme ultraviolet (EUV) lithography at 13.5 nm [8]. This progression has enabled micro- and nanofabrication to advance from the micromoter scale to 7 nm and even below 5 nm. This technology has had profound impacts on other fields, such as

mechanical engineering, where micromechanical devices (e.g., micromotors and microactuators) perform functions traditionally handled by large equipment in very small spaces, and are widely used in micromechanical systems, accelerometers, gyroscopes, digital micromirror devices (DMD) [9], Lidar [10], microsurgical instruments [11], and microfluidic devices [12].

Furthermore, advancements in micro- and nanofabrication have enhanced our understanding of micro- and nanoscopic forces, such as van der Waals forces [13], Casimir forces [14], and nanoscale friction [15]. They have also driven advancements in optics, leading to development in micro-lasers (Micro-LEDs) [16], microlenses [17], micro-optical sensor [18], and optical waveguides [19]. These technologies not only improve device performance but also drive progress in cutting-edge fields such as optical communication, display technology, medical devices, and autonomous driving.

In the last few decades, scientific research has increasingly shifted from the macroscopic scale to the micro- and nanoscale, where materials often exhibit properties that differ significantly from those observed at large scales [20]. For example, nanoparticles can show unique color changes due to size effects. These distinctive properties of micro- and nanomaterials arise from quantum effects and surface effects [21], which are typically not visible at the macroscopic scale. Consequently, research at the micro- and nanoscale has become a key frontier in modern science. A key challenge is overcoming the Brownian motion of micro- and nanoobjects to achieve precise control and study of their physical and chemical properties. Brownian motion leads to the random movement of micro- and nanoparticles within a fluid, complicating their manipulation and observation. Therefore, researchers need to develop technologies capable of effectively controlling and manipulating micro- and nanoobjects to accurately measure and understand their behavior and properties at this unique scale.

The advancements in microfabrication techniques driven by the development of integrated circuits provide a crucial technological foundation for research at the micro- and nanoscale. Advanced microfabrication techniques make it possible to construct complex optical and mechanical structures on chip, in turn, facilitating precise control of objects at micro- and nanoscale. For example, the optical enhancement provided by plasmonic structures formed by on-chip nanostructures can enable the trapping of particles as small as few nanometers [22,23], overcoming the limitations of traditional optical tweezers. With the aid of these advanced fabrication techniques, research has evolved from simple particle trapping and manipulation to imparting intelligence to micro- and nano-objects, ultimately leading to the development of multi-functional microrobots. Integrating photovoltaic cells, micro-actuators, and even micro-circuits into robots with dimensions of hundreds of micrometers enables capabilities such as locomotion on flat surfaces [24], programmable behavior [25], and the ability to mimic ciliary action for microfluidic control [26].

Following a brief introduction, I will demonstrate how I apply microfabrication techniques—such as thin film deposition, photolithography, and etching—to fabricate chips for studying torque generated by the forces occurring at the micro- and nanoscale. I will also show how this torque is used to manipulate microfabricated disk particles and colloids, typically a few micrometers in size. Additionally, I will discuss the fabrication of nanophotonic structures that impart intelligence to particles, enabling them to exhibit complex swimming behaviors in liquid under optical illumination. These particles are then integrated into chips to create functional on-chip micromachines, which are applied

to fluid control. For more details, for each study performed during my PhD, i will present: a short motivation, the current state-of-the-art, the aim of the study, and at last the main results found.

1.1 Nanoalignment by critical Casimir torques

The manipulation of microscopic objects, such as colloids and nanoparticles, is crucial across various research fields, including nanotechnology [27, 28] and materials science [29, 30]. However, controlling these micro- and nanoparticles presents significant challenges due to thermal fluctuations present in the environment. To address these challenges, external physical fields, such as magnetic [31–35] optical [23, 36–39] and electric [40–44] tweezers, are employed to control particle movement. Nevertheless, these methods face limitations in achieving precise and scalable manipulation, as well as in configuring and aligning particles. Recently, critical Casimir forces — arising between micrometer-sized objects due to phase transitions in binary liquids induced by external temperature changes — have attracted considerable interest [45]. These forces can be either attractive or repulsive depending on the wetting properties (hydrophilic or hydrophobic) of the objects [46, 47]. Utilizing these properties, critical Casimir forces have been employed for particle assembly to create new matter [48] and study their physical and chemical physical and chemical phenomena [49], and overcoming the quantum electrodynamic (QED) Casimir forces in MEMS devices to mitigate stiction issues [50]. Despite these advancements, the potential of critical Casimir forces remains largely unexplored in comparison to Casimir forces, especially concerning the use of critical Casimir forces to manipulate the movement of microparticles [50–52].

Here, I employed microfabrictation techniques such as photolithography and film deposition to construct a large-scale periodic substrate. The substrate is composed of a fused silica (SiO_2) base with a 25-nm-thick patterned gold film deposited on its surface. By functionalizing the gold with thiols, the gold regions were made hydrophobic, while the SiO_2 regions remained hydrophilic. The substrate was used to trap 3 µm colloidal and 2.4 µm disk particles by critical Casimir forces, which arise near the critical point of a phase transition in binary liquids. The disk particles were also fabricated by microfabrication techniques. A novel configuration was discovered, where the disks align vertically with respect to the patterned substrate, resulting from the balance between attractive and repulsive critical Casimir forces, electrostatic force and gravity. By adjusting the design of the substrate, the critical Casimir torque was exploited to manipulate the orientation of these disk particles while maintaining their vertical configuration. Beside particle trapping, the critical Casimir force was utilized to create a Brownian ratchet, where the magnitude of the force — correlated with the interaction area between the particles and the underlying pattern — was regulated by modifying the area of pattern. This allowed for the control of particle movement, enabling both straight and curved trajectories. Combing temperature-controlled open-loop systems with a series of microfabricated patterns to generate multiple Brownian ratchets, the particles were directed over long distances in a defined direction. Finally, I demonstrated that the critical Casimir torque can be employed for the selective trapping of chiral particles, where particles were trapped only when the chirality of the pattern matched that of the particles. A detailed exploration of these finding is provided in Section 4.1 and **Paper I**.

1.2 Light-Driven Microswimmer with Complex Behavior

Considerable progress has been achieved in manipulating micro- and nanoparticles in liquids by overcoming Brownian motion through the application of external fields. A promising area of research is the development of self-propelled particles, known as microswimmers, which can harvest energy from their surroundings for autonomous motion. These particles emulate biological systems like bacteria and hold potential for applications in biomedicine for targeted drug delivery and in environmental remediation for pollutant degradation. Most current microswimmers utilize a Janus structure, where one side is coated with materials that respond to chemical [53–56], electric [57–59], magnetic [60–63], acoustic [64–66] or optical fields [67–70], facilitating directed propulsion. However, this design restricts their range of behaviors. While manipulating external fields can induce complex behaviors, it often makes the particles resemble puppets, thereby diminishing their autonomy. The long-term goal is to create intelligent particles that can autonomously exhibit a variety of complex motion trajectories in stable external fields without external control. Yet, designing and fabricating these microswimmers based solely on simple principles under a single field — rather than relying on the integration of multiple physical fields — presents significant challenges.

To address this challenge, I drew inspiration from some previous work on using light metasurfaces to drive metavehicles [71]. By employing traditional photolithography techniques, I embedded the same metasurface into microswimmers of identical shape but with varying metasurface distributions. This approach creates asymmetric force distributions that generate optical torque, causing the swimmers to rotate along circular trajectories. By adjusting the amount of metasurface on each swimmer, I can control the torque, enabling the particles to exhibit elliptical motion. Additionally, altering the metasurface orientation regulates the direction of rotation. The shapes of the particles can also be freely modified, resulting in a diverse array of motion trajectories. Furthermore, the particles respond to polarization; dynamically adjusting the light's polarization reveals even more complex trajectories. A detailed exploration of these finding is provided in Section 4.2 and **Paper II**.

1.3 Light-Driven Micromachines

Although our light-driven microswimmers demonstrate diverse behaviors and can be fabricated into various configurations using microfabrication techniques, their operation is confined to liquid environments. In such media, their motion becomes random and influenced by external factors when illumination is removed, making it challenging to couple them into complex systems capable of performing sophisticated tasks. While optical [72] and optoelectronic tweezers [73] can facilitate coupling, these methods are unstable without continuous illumination. Therefore, developing on-chip integration methods is essential.

To address these limitations, we have developed a novel fabrication process that integrates rotational microswimmers into glass chips using three-dimensional structures, enabling stable on-chip rotation. Using the high precision of semiconductor photolithography, we have achieved the coupling of multiple micromotors to construct microscopic

geared mechanisms with sizes well below 100 µm. This represents a significant advancement, as conventional semiconductor techniques for electrostatic or mechanical actuation are typically limited to dimensions down to a fraction of a millimiter. While far-field methods such as magnetic or electric fields can further miniaturize systems, they require specialized responsive materials, complicating the integration of heterogeneous components and their compatibility with existing microfabrication processes. Optical tweezers, constrained by the need for localized light fields, are limited in scalability and are primarily suited for manipulating single motors rather than complex multi-motor systems.

In contrast, our use of metasurfaces, which are compatible with CMOS fabrication processes, provides greater flexibility in designing complex on-chip architectures. This approach enables the construction of microscale systems that exhibit mechanical advantages, such as speed and torque amplification, similar to those found in macroscopic mechanical systems. Operating under linearly polarized 1064 nm laser illumination, these devices allow for precise control of rotation speed through adjustment of light intensity. Furthermore, the circular polarization of light was used to dynamically control the rotation direction of motors, allowing for advanced manipulation capabilities. Beyond rotational motion, the integration of gears and racks facilitates the conversion of rotation into linear movement, expanding the functionality of these devices. A detailed exploration of these finding is provided in Section 4.3 and **Paper III**.

1.4 Micromotor-Assisted Optofluidics

Once miniaturized rotary motors and functional machines have been developed and fully integrated into chips, the next step is to employ them for applications. The manipulation of microfluidic flows facilitates the handling of micro- and nanoscale objects, which is essential, for example, for drug screening [74,75] and chemical reaction [76,76]. A key goal in this field is the creation of fully integrated automated liquid handling systems that can replace traditional, bulky fluid-driving devices such as pumps [77–79]. Recent research has focused on light-driven mechanical components to facilitate this advancement, as they can operate effectively within narrow fluid channels. However, these systems typically rely on focused, high-intensity light [80], which restricts their scalability. Although structured light devices can address this limitation, they require feedback control [73, 81], increasing overall complexity. Additionally, light-driven systems are normally constrained by specific geometries, which limits their applicability. The chip integrated metasurface-driven micromotors in **Paper II** work under plane wave illumination and are not constrained by specific configurations, effectively overcoming these limitations.

I investigated the effects of individual motor rotation on the surrounding fluid field, using SiO_2 particles as tracers to map flow patterns and validate the results through simulations. High-precision photolithography enabled the fabrication of motors with varying inter-motor distances. By adjusting the metasurface orientation, motors rotating in opposite directions were integrated on the same chip, replicating the function of traditional pumps. The fluid field exhibited linear and curved flows depending on the motor arrangement, allowing for precise manipulation of fluid dynamics. To demonstrate the platform's potential for reconfigurable fluid control, I constructed a 4x4 motor array where the rotation direction of each motor could be defined. This configuration generated linear,

rotational, and reciprocating flow fields, as well as more complex flow patterns. Additionally, by controlling circular polarization of light, integrated microfluidic valves and pumps were created, enabling reconfigurable control of fluid motion. A detailed exploration of these finding is provided in Section 4.3 and **Paper IV**.

1.5 Thesis Outline

This thesis is structured into six chapters, each addressing a different aspect of my research:

Chapter 2 provides the background for the work conducted in this thesis, focusing on the key research fields that are most relevant to my research. It also discuss the current limitations and challenges in these fields, which serve as the motivation for the research presented here.

Chapter 3 gives an overview of the research tools and methodologies employed throughout my experiments. This chapter describes the fundamental principles behind these tools, facilitating a clear understanding of the experiments conducted and the technical approaches implemented in the research.

Chapter 4 offers a detailed account of the research I conducted during my PhD. This chapter focuses on summarizing the key findings from each research projects, specifically highlighting my contributions to each study.

Chapter 5 draws conclusions from the research carried out over the PhD. It also provides insights into potential future research directions and how the work presented here can be expanded upon in subsequent studies.

Chapter 2

Background

The focus of **Papers I–IV** is the application of microfabrication techniques to develop micro- and nano-structures for controlling microparticle behavior. This chapter provides a brief overview of the background for the research presented in each paper. I begin by reviewing key principles of physical gradients such as magnetic, electric, acoustic, optical, and thermal fields used to overcome Brownian motion in passive particles and enable precise movement control. The advantages, limitations, and practical applications of these approaches are discussed. I then introduce the principle and application of the critical Casimir force, controlled by temperature, as applied in **Paper I** to manipulate passive particle movement. Next, I discuss active particle systems, specifically microswimmers, which can harness energy from their environment. I provide an overview of various types of microswimmers that use magnetic, optical, chemical, or electric fields for self-propulsion. A specific focus is on light-driven microswimmers using nanostructures to modify the light field, as explored in **Paper II**. Building on the background of **Paper III**, I present various micromotors that differ from microswimmers by achieving rotational motion through external physical fields. Finally, I introduce the research on using motors for fluidic manipulation, which serves as the background for **Paper IV**.

2.1 Micro- and nanoparticle manipulation approaches

When microscopic particles are observed under a microscope, it becomes evident that they do not remain stationary [82]. Whether these particles are dust motes floating in sunlight or colloidal particles suspended in water, they exhibit a continuous, erratic motion. This phenomenon is termed Brownian motion, named after the botanist Robert Brown, who first documented it in 1827. Brownian motion is characterized by the random thermal movement of particles suspended in a fluid, driven by their interactions with the fluid molecules. These collisions are isotropic and non-uniform, resulting in unpredictable trajectories. Large particles, due to their greater mass, exhibit less pronounced Brownian motion, while micro- or nanometer-sized particles are more significantly perturbed by thermal agitation, resulting in more noticeable random movement. This phenomenon is quantitatively described by the mean squared displacement (MSD), which measures the average squared distance that particles travel over time. The MSD is given by

$$\langle \Delta r^2(t) \rangle = 6Dt$$

where $\langle \Delta r^2(t) \rangle$ represents the MSD, and D is the diffusion coefficient. The diffusion coefficient D is determined by

$$D = \frac{k_B T}{6\pi\eta r}$$

Here k_B is the Boltzmann constant, T is the temperature,η is the fluid's dynamic viscosity, and r is the particle's radius. This relationship shows that smaller particels, with their smaller radius r, experience higher diffusion coefficients and thus exhibit more pronounced Brownian motion. Conversely, higher fluid viscosity (η), reduces the diffusion coefficient, affecting particle movement [83, 84]. Fig. 2.1a shows the Brownian of a disk-shaped particle.

Overcoming Brownian motion is crucial for the precise manipulation of micro- and nanoparticles, with broad implications across scientific and technological fields [27, 28, 85, 30,86,29,87–89]. For example, controlling motion of particles allows for the investigation of fundamental physical phenomena at microscopic scales, such quantum effects [85, 90] and nanoscale interactions [91, 92], and facilitates the development of advanced materials with tailored properties. Additionally, it enables the precise manipulation of cells [93, 94] and biomolecules [95, 96], which accelerates drug discovery and enhances our understanding of cellular processes. Thus, effectively overcoming Brownian motion to manipulate micro- and nanoparticles is fundamental to advancing research and applications across diverse scientific domains.

The manipulation of micro- and nanoparticles is commonly performed through the application of external fields [97–99], which create gradients to control their movement and orientation. These fields can be magnetic [31–35], optical [36, 23, 37–39], electric [40–44], acoustic [88, 100–103], or temperature [104–108], each providing a different approach for controlling the particle dynamics.

Magnetic fields are commonly employed to manipulate magnetic objects, providing a versatile and non-contact method of control. The field can be generated using coils [109], which produce magnetic fields of varying directions and strengths by adjusting the electric current flowing through them, or permanent magnets [110], which offer a constant magnetic force and can physically move or position objects. Coils are particularly useful for dynamic applications, as the magnetic field they generate can be precisely controlled and modulated in real time, while permanent magnets are more suitable for stable, fixed operations [111]. Magnetic fields are commonly used for the separation and purification of biomolecules, such as proteins, DNA, and cells [112, 113], as well as for studying physical and chemical phenomena at the single-molecule level by manipulating magnetic particles [114, 115]. As shown in Fig. 2.1b, magnetic tweezers are used to study the polymerization kinetics of a catalyst-driven ring-opening metathesis polymerization (ROMP) reaction. The growing polymer chain is tethered at one end to a magnetic particle and anchored at the other end to a substrate. A magnetic field are used to trap the particle and applied force to move it along the Z-axis. As the chemical reaction extends the polymer chain, real-time tracking of the particle's position provides insight into the polymer growth kinetics [31].

Similar to magnetic fields, the manipulation of micro- and nanoparticles of electric fields is based on the interaction between the particle and electric fields such as dielectrophresis [116, 117], electrophoresis [118], electro-osmosis [119] and electro-rotation [120]. Dielecrtophoresis (DEP) is the force experienced by neutral particles in a non-uniform

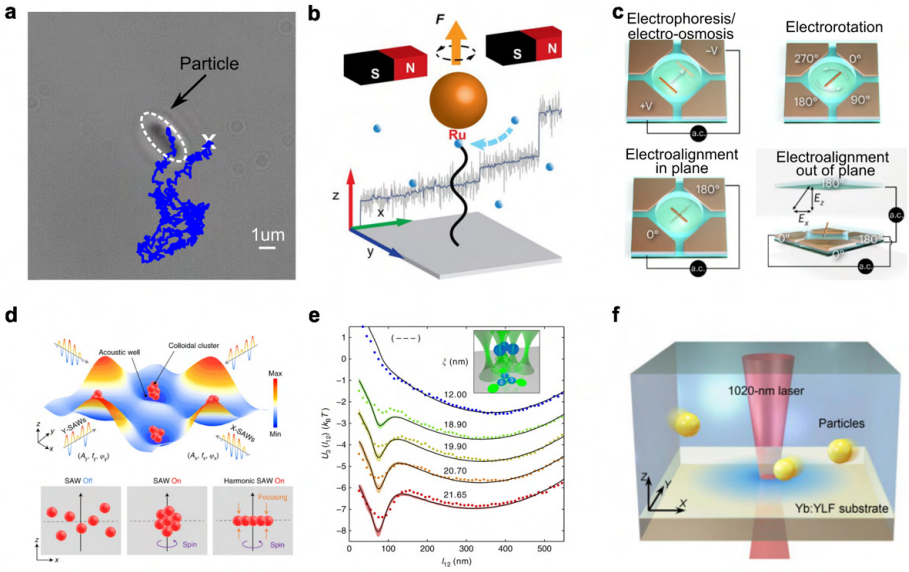

Figure 2.1: Particle manipulation by overcoming Brownian motion using various approaches. **a** Trajectory of disk-shaped particles in solution due to Brownian motion. Scale bar: 1 µm. **b** Schematic of magnetic tweezers. A magnetic particle, attached to a growing polymer chain, is trapped and pulled upward by magnetic forces. The particle is connected to a catalyst that inserts new monomers (blue spheres), causing the polymer to extend [31]. **c** Electrokinetic effects, such as electrophoresis, electroosmosis, and electrical alignment both in-plane and out-of-plane, are used to control the transport and orientation of nanorods [42]. **d** Schematic showing colloidal clusters confied within acoustic wells through the application of surface acoustic waves (SAWs) along the x and y axes. Below, an illustration depicts the formation of a colloidal crystal monolayer by vertically concentraing particles using harmonic SAWs [88]. **e** The optical tweezer is utilized to trap multiple particles and investigate the non-additivity of the critical Casimir force between them. The interaction between the particles is represented by the potential as the system's temperature approaches the critical point of a binary liquid solution [37]. **f** Schematic of the localized laser cooling process on the substrate and the resulting thermophoretic trapping of particles at the cold region [104]. Images (**b-f**) are reproduced with permission from Refs [31, 42, 88, 37, 104]

electric field, influenced by their polarizability. Polarizability is determined by the dielectric constant and conductivity of both the particle and the surrounding medium [121]. When exposed to an electric field, particles become polarized, with the extent of polarization indicating the charge distribution relative to the medium. Particles with a higher dielectric constant or conductivity than the medium experience positive dielectrophoresis, moving toward regions of higher electric field strength. Conversely, particles with a lower dielectric constant or conductivity exhibit negative dielectrophoresis, moving toward regions of lower electric field strength. Electrophoresis is a process in which charged particels migrate under the influence of an electric field. The field generates Coulombic forces that drive the particles along its direction. Positively charged particles move towards the negative electrode, while negatively charged particles travel towards the positive electrode. Electro-osmosis is the movement of liquid along a solid surface driven by an electric field. When the liquid interacts with a charged solid surface, it creates an electrical double layer: a fixed layer of charge on the solid and a mobile layer of ions in the liquid. The application of an electric field exterts electrostatic forces on the ions in this double layer, which drives the flow of the liquid. Electrorotation describes the rotational motion of particles subjected to an alternating electric field due to asymmetric polarization effects. When an alternating electric (AC) field is applied, it induces varying plarization forces on the particle throughout different phase f the field, leading to rotational movement. This effect arises from the interaction between the electric field-induced dipole moment of the particel and non-uniform forces exerted by the electric field. These effects combine to enable precise manipulation of micro- and nanoscale particles and are utilized in applications such as particle separation and trapping. For example, in the chamber configuration shown in Fig. 2.1c, a multifunctional trap can be developed by integrating dielectrophoresis, electroosmosis, electroalignment, and electrorotation. Utilizing a closed-loop feedback control system with direct current signals applied to four planar motors allows for precise two-dimensional control of nanowire positioning. Alternating current signals facilitate the alignment and orientation of nanowires through electrorotation [42]. This approach, combined with digital microscopy imaging, permits real-time monitoring of nanowire position and orientation, while proportional-integral control is employed to correct and adjust deviations from the target settings.

Compared to magnetic and electric fields, which require the material components of particles to respond to magnetic or electric fields and impose restrictions on the properties of particles, acoustic field manipulation has relatively lower requirements on the properties of the particles [122]. Acoustic waves exert forces on objects via acoustic radiation force, generated by pressure gradients as the waves interact with the object [123, 124]. As the waves propagate, they induce local pressure changes in the medium [125], causing forces on particles. The strength and direction of this force depend on the particle's density, compressibility, and contrast with the surrounding medium [125]. In uniform waves, particles move along the wave's path, while in non-uniform or standing wave fields, forces act from multiple directions. Standing waves, formed when two waves of the same frequency travel in opposite directions, create stable pressure nodes and antinodes. Particles move toward nodes (positive force) or antinodes (negative force), allowing for particle trapping [88,126]. Acoustic waves can also suspend objects through acoustic levitation [127], where standing waves between two reflectors balance gravitational and acoustic forces, holding the object at pressure nodes. In Fig. 2.1d, an AC voltage is applied to photolithographically pat-

terned interdigital transducers, generating surface acoustic waves (SAW) on a piezoelectric chip to create a programmable platform for colloid and cell manipulation. The platform operates by combining two independently programmable SAW waveforms, allowing precise and selective control of colloids and cells through arbitrary waveform patterns. Beside that, acoustic waves can also be used to manipulate particles for 3D printing [100, 128].

While the manipulation of particles by magnetic, electric and acoustic fields is generally implemented on a large scale, achieving precise manipulation over individual objects remains a significant challenge [124]. Light field, such as optical tweezers, present a promising solution for addressing this issue by enabling precise manipulatio of single particles with the size range from atoms [129], molecules [130] to micro particles [5]. Optical tweezers use a highly focused laser beam to exert forces on micro- and nanoparticles, enabling their manipulation and trapping. When a laser is focused on a particle within a transparent medium using a high numerical aperture (NA) lens, the interaction between the particle and the electromagnetic field creates a force that drives the particle toward the focal point, where the light intensity is highest.The force acting on the particle in that can be divided into two types: scattering/absorption forces ($F_{\mathrm{scat/abs}}$) and gradient forces (F_{gra}) [39]. Scattering/absorption forces result from momentum changes when photos interact with the particle, typically pushing it along the direction of the light beam. The gradient force, on the other hand, is produced by the variation in light intensity around the particle, pulling it toward the focal point. This gradient force is essential for stable particle trapping. when gradient force surpasses the scattering/absorption forces, the particle remain securely trapping at the focus point of beam. In addition to the successful applications of optical tweezers in biophysics [95], one of their most significant uses is in manipulating colloidal particles and studying the interactions between them [131]. In Fig. 2.1e, holographic optical tweezer is used to trap micro-sized spheres and measure the critical Casimir force between them, which is inducedd by density fluctuations resulting from phase transitions in binary liquid system. The generation and modulation of this force can be monitored by dynamically varying the temperature while keeping the particles in a trapped configuration. The magnitude of optical force is usually in the femtonewton (fN) and piconewton range, and since high-focused energy beams usually cause damage to bilogical sample, some methods that rely on light to cause changes in electric fields [94,132,133] and heat [105, 105] in the environment are also used to achieve the manipulation of micro- and nanoobjects, such as optoelectric tweezers and opto-thermoelectrci tweezers.

In addition to traditional methods like electric, magnetic, acoustic, and light fields, temperature-based particle manipulation is emerging as a new research direction. Unlike other technique, temperature manipulation offers broad applicability across materials, as it does not depend on specific electrical or magnetic properties [105, 134]. For example, in Fig. 2.1f, using laser to excite a substrate results in short-wavelength emission, which induces cooling in the crystal and generates a low-temperature region at the excitation spot. This creates a temperature gradient that facilitates the manipulating of various types of particles, including polystyrene (PS) nanoparticles and biological proteins [104]. Temperature via heat can also induce phase transitions [50] or chemical reactions [135], altering their behavior in ways that are not achievable through other manipulation techniques. Importantly, it eliminates electromagnetic interference, making it particularly advantageous in sensitive environments such as biomedical [136] and nano-electronics applications [87]. Recent research has primarily focused on the use of lasers to heat metals or light-absorbing

materials, generating localized temperature gradients that induce thermophoresis for particle trapping. However, this method is constrained to small areas due to the difficulty of sustaining stable temperature gradients over larger regions, limiting its application to micro- and nanoscale systems. Large-scale manipulation remains an unresolved challenge.

In **Paper I**, I address this challenge by demonstrating large-scale trapping and manipulation of disk- and sphere-shaped colloidal particles through temeprature modulation of the system, leveraging the critical Casimir force generated by density fluctuations in the binary liquid at the critical temperature, driven by a temperature induced liquid-liquid phase transition.

2.2 Particle manipulation by critical Casimir force

In solution systems composed of two different liquids, uniform mixing is not always observed. For instance, while some liquids, such as water and acetone, mix thoroughly, others, like oil and water, tend to separate into distinct phases. The mixed state is thermodynamically favored because it leads to higher entropy, which stabilizes the system. Conversely, phase separation occurs when similar molecules cluster together, reducing the system's energy [137]. In systems like water and 2,6-lutidine solutions, both mixed and demixed states can manifest, depending on temperature and the composition ratio of the mixture. The phase diagram (Fig. 2.2) illustrates this transition, with the white region representing a mixed state and the blue region indicating phase separation. A single boundary separates these states, and within this boundary, both phases coexist. In this region, droplets form, with each phase containing a small amount of the other. For example, a higher concentration of 2,6-lutidine results in water-rich droplets, while an increased concentration of water leads to lutidine-rich droplets, with droplet sizes increasing over time. Crossing this boundary results in complete phase separation. Temperature plays a crucial role in this process, as the transition from mixing to separation requires overcoming an energy barrier.

An interesting phenomenon occurs at the critical point of the phase transition in a binary liquid, as indicated by the red points in Fig. 2.2. As the system approaches this point, local density fluctuations arise, with the correlation length and relaxation time intensifying and eventually diverging at the critical point [139]. A more intuitive understanding is that the solution composed of water and 2,6-lutidine continuously undergoes demixing and remixing across different time and length scales, influenced by the temperature difference. These fluctuations originate at the molecular level and gradually develop to the microscopic scale. When these fluctuations are confined between the surfaces of two objects, which can be either plates or spheres, a force known as the critical Casimir force is generated (Fig. 2.3a). This force is analogous to the quantum electrodynamics Casimir force, which was predicted by Hendrik Casimir in 1948. When quantum electrodynamic vacuum fluctuations are spatially confined between two surfaces, such as uncharged conducting plates, the difference between the internal and external fluctuation modes lead to an attractive force between the plates [140]. This force is widely observed in microelectromechanical systems (MEMS) [141, 142] and depends on the dielectric constant and magnetic permeability of the materials involved allowing the Casimir force to be either attractive or repulsive [143, 144]. Similarly, the critical Casimir force can be either attractive

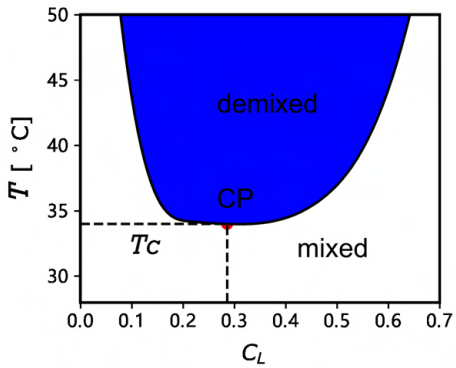

Figure 2.2: Phase diagram of the water-2,6-lutidine mixture. In the mixture of water and 2,6-lutidine, a lower critical point (CP) is observed at the base of the coexistence line (solid line). This mixture is created at a critical lutidine mass fraction of $C_c = 0.286$, which correlates with a critical temperature of $T_c \approx 34°C$. The data presented are sourced from Refs. [138].

or repulsive depending on whether the boundary conditions are symmetric. The boundary conditions are determined by the preferences of the surfaces for the solution components. In the water and 2,6-lutidine system, this manifests as wettability, which includes both hydrophilic and hydrophobic. When both surfaces exhibit the same wettability, such as being hydrophilic, an attractive force is observed; conversely, when the wettability differs, a repulsive force is exhibited.

The theoretical prediction of the critical Casimir force was completed by Fischer and de Gennes in 1978 [139]. Subsequently, in 2008, experimental measurements of the critical Casimir force were conducted [46]. Specifically, a single colloidal sphere and a flat substrate were immersed in a binary solution of water and 2,6-lutidine. The force generated between the two objects was measured in situ with a resolution of femtonewtons (fN) using total internal reflection microscopy. Chemical treatment of the substrate allowed it to become charged, thereby altering its wettability and enabling the adjustment of whether the critical Casimir force was attractive or repulsive. The maximum measured attractive force was approximately 600 fN, comparable to the reported quantum electrodynamic Casimir force [146]. Following this, optical tweezers were utilized to measure the critical Casimir force between multiple colloidal sphere [37], exploring the many-body effects of this force and yielding results similar to those found in Casimir force [147]. Due to the tunability of this force with temperature and surface properties, it can be employed to study the self-assembly of colloidal particles. For instance, the critical Casimir force can induce colloidal particles to assemble into liquid-like and solid-like phases under temperature modulation [48]. Furthermore, patterned colloidal particles can be likened to atoms in a model that uses the critical Casimir force to assemble into phenyl ring molecules [148] or graphene analogs [49], allowing for investigations into the effects of defects on material properties.

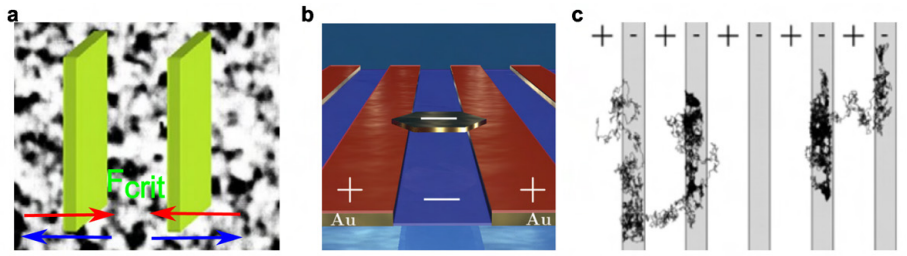

Figure 2.3: Critical Casimir force on pattern substrate. a Two plates immersed in a binary liquid experience critical Casimir force due to the density fluctuations at the critical point. The critical Casimir force can be either attractive (red arrow) or repulsive (blue arrow). **b** A gold disk moves over a periodic pattern composed of gold and glass. The '+' sign indicates hydrophobic surface wettability, resulting from function of thiols on the gold surface, which leads to a critical repulsive force at the critical point. Conversely, the '-' sign indicates hydrophilic properties, resulting in a critical attractive force at the critical point [50]. **c** At the critical point, hydrophilic (-) polystyrene (PS) particles remain on the hydrophilic (-) surface for an extended duration due to the critical Casimir attractive force, while they stay on the hydrophobic (+) surface for a shorter time [52]. Images (**a-c**) are reproduced with permission from Refs. [50, 52, 145].

A more practical application of the critical Casimir force involves overcoming the quantum electrodynamic Casimir force (Fig. 2.3b), as the attractive Casimir force in MEMS devices can often be detrimental and lead to device failure. By modifying a gold surface with a layer of thiols, it can exhibit hydrophobic when immersed in a binary liquid solution. At the critical temperature, the resulting critical Casimir repulsive force can counteract this attractive force, thereby mitigating the adverse effects of device deactivation [50]. This method of modifying surface wettability with organic molecules to regulate the critical Casimir force is also essential for the studies presented in **Paper I**. This approach is not confined to surfaces with a single wettability characteristic. substrate exhibiting both hydrophilic and hydrophobic properties can direct the aggregation of colloidal particles and enable control over their movement [52], as shown in Fig. 2.3c. In **Paper I**, I used microfabrication techniques, including photolithography and etching, to create patterned substrate that harness temperature-tuned critical Casimir forces to trap and manipulate particle motion.

2.3 Microswimmer self-propulsion approaches

For the manipulation of micro- and nanoparticles, in addition to employing physical fields (such as electric, magnetic, or light field) to generate gradients for trapping and controlling their movement, the configuration of the particles can be engineered to enable them to harness energy from their surrounding environment or external fields [149, 150], facilitating autonomous movement. These self-propelling particles are referred to as "active microswimmers," with natural examples such as bacteria, which use flagella (Fig. 2.4a) or other motility structures to extract energy from their environment and propel themselves through fluid media [151–153]. Here, we will primarily focus on artificial active microswimmers.

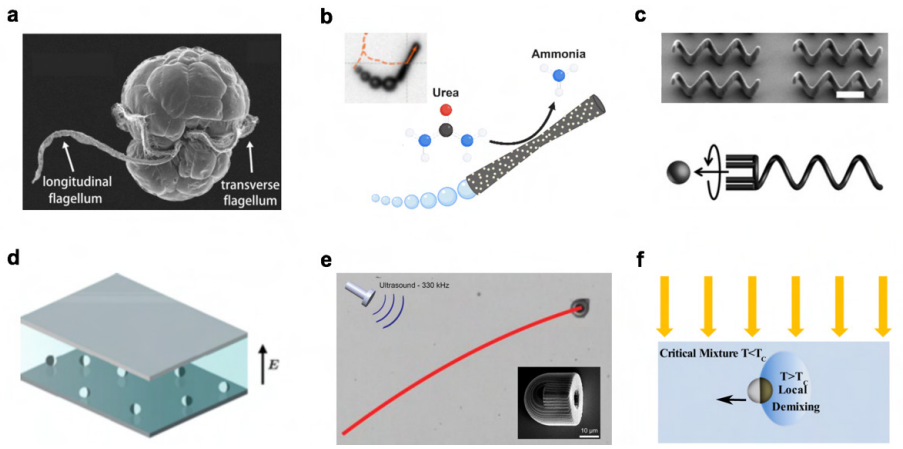

Figure 2.4: Microswimmer self-propulsion based on different approaches. a Scanning electron microscopy (SEM) image of *E.voratum* with its flagella [154]. **b** MnO_2 tubular micro-swimmers, modified with laccase, exhibit propulsion through the generation of bubbles resulting from the oxidative reaction of organic substrates. The inset displays a microscopic image capturing their motility [155]. **c** A magnetic field-driven helical microswimmer, with nickel deposited on its surface, demonstrates responsive behavior to an applied magnetic field. The top image displays the scanning electron microscopy (SEM) image of the swimmer, while the bottom image illustrates the swimmer's ability to capture a oobject while navigating in a rotating magnetic field [60]. **d** Janus microswimmers are driven by a vertical electric field generated between two ITO glass slides [156]. **e** A hemispherical microswimmer operating under ultrasound captures air bubbles in its spherical cavity, enabling movement. The inset displays its SEM image [64]. **f** Janus microswimmer half-coated with light-absorbing materials absorb light and generate heat, causing asymmetric temperature rise. This triggers a phase change in the solution and creates a concentration gradient that drives microswimmer movement [157]. Images (**a-f**) are reproduced with permission from Refs. [154, 155, 60, 156, 64, 157].

Different types of artificial active microswimmers can be classified according to the external fields from which they derive energy, such as chemical [53–56], electric [57–59], magnetic [60–63], acoustic [64–66], and light fields [67–70]. Among the various types, chemically powered microswimmers, which mimic natural systems by extracting chemical energy from their environment and converting it into motion via chemical reactions, are typically designed as Janus particles. These colloidal particles have an asymmetric structure, with one hemisphere coated with catalytic metals or metal oxides, such as platinum (Pt) [158], manganese dioxide (MnO_2) [159], or gold [160]. The catalytic part of the particle interacts with environment chemicals, typically through redox reactions or catalytic decomposition. These reactions consume the surrounding chemicals and produce gases or other byproducts, leading to the development of a local pressure gradient around the particle. This pressure gradient generates a force that propels the particle through the liquid, enabling self-propulsion. In Fig. 2.4b, MnO_2 tubular microswimmers, functionalized with the enzyme laccase, demonstrate propulsion via the generation of bubbles. This propulsion is driven by oxidative reactions involving organic substrates [155].

Microswimmers driven by chemical reactions typically face challenges in precisely controlling their direction and reaction speed in real time [161]. While light can be used to induce these reactions and enhance precision [162–164], the effectiveness is still limited by the chemical environment. External fields, such as electric, magnetic, and light fields can avoid this limitation. Among these, magnetic fields are the most commonly used because they penetrate tissues more effectively than electric or light fields and can be applied within living organisms for applications such as drug delivery [61,165]. Magnetic fields are typically generated by coils [109]. By varying the number and orientation of these coils, different types of magnetic fields such as alternating, rotating, and gradient. This enables precise control over the microswimmer's direction and velocity. Additionally, optimizing the design of the microswimmer can increase its velocity and enhance its ability to navigate through viscous fluids [60, 166, 167]. As illustrated in Fig. 2.4c, the helical microswimmer is fabricated by direct laser wrting on a negative photoresist to form its shape. A thin Nickel/Titanium double layer is then deposited on the surface of swimmer. When exposed to a rotating magnetic field, the microswimmer exhibits exceptional motility in both water and serum, with its helical propulsion significantly reducing frictional drag from the liquid and enabling efficient cargo transport [60]. This design has shown potential application in sperm screening and the treatment of eye diseases.

An AC electric field is similar to a magnetic field but generally involves simpler setup that typically consist of two conductive glass slides coated with indium tin oxide (ITO) [156]. The microswimmer used are typically Janus particles, where one side is coated with a conductive metal layer. When exposed to the external electric field, these particles induce surface charges that create an asymmetric distribution. This leads to electrophoretic effects that propel the particles through the liquid (Fig. 2.4d). Furthermore, the AC electric field generates rotational torque that aligns the particles' axes perpendicular to the field direction, which is the most stable configuration and results in directed movement. Due to interactions between induced charges on different microswimmer, AC electric field-induced microswimmers are employed to study the collective behavior at micro-scale [58, 59].

Acoustic fields are combined with chemical [161], magnetic fields [168] et.al as source of propulsion or directional control for microswimmers. The principle is that when acoustic

waves passes through a liquid, it generates acoustic waves that produce radiation forces on microscopic objects, which propel the microswimmer forward or alter its direction. Precise control over the microswimmer can be achieved by adjusting the frequency, intensity, an direction of the acoustic waves [169]. Fig. 2.4e shows a hemispherical microswimmer that has a diameter of 24 µm and is fabricated using two-photon polymerization (2PP). It contains a spherical cavity that captures air bubbles and moves at a speed of 90 body lengths per second (2250 $\mu m/s$) under the influence of acoustic waves. The head is coated with a soft magnetic nanofilm that enables its motion to be controlled by a magnetic field [64].

Light is widely used to power the movement of microswimmers due to its ability to focus into small spots with optical components like lenses and commercial devices such as digital micromirror devices (DMD) [170], spatial light modulators (SLM) [171], and acousto-optic deflectors (AOD) [172]. These systems provide both more precise individual control and the ability to manipulate multiple microswimmers in parallel compared to other methods, while maintaining a non-invasive approach [173]. Microswimmers are propelled by optical forces using optical tweezers to manipulate different parts of the swimmer, with movement controlled by adjusting the position of the optical field relative to the environment. These microswimmers are fabricated in various configurations using two-photon lithography [174], allowing for feedback control of functional behaviors such as cell capture, transport [175], or surface scanning with optical probes [176]. In addition to optical force, light-driven microswimmers typically operate by converting optical energy into thermal [69, 157] or chemical reactions [162–164]. For instance, Janus particles perform in the binary liquid with one side made from a light-absorbing material (Fig. 2.4f). At low temperature, the liquids mix uniformly. Upon illumination, the absorbed light converts to heat, causing a localized temperature increase that induces phase separation and creates a concentration gradient, which drives the linear motion of the microswimmer [157]. Besides that, the microswimmers perform rapid rotation under focused laser beam [177]. This light-to-heat conversion not only drives rigid microswimmers but also induces deformation in soft materials such as hydrogels, enabling swimming behavior [68]. Furthermore, numerous microswimmers are driven by light-induced chemical reaction, including azobenzene cis-trans isomerization [178] and photocatalytic decomposition of reactants [163], which generate chemical propulsion.

Although optical driven microswimmer have been extensively studied, several challenges remain. Optical tweezers-driven microswimmers typically require highly focused laser beams to generate optical gradient forces. This requirement limits their scalability, and such systems resemble a marionette, with the microswimmer's position being dependent on the location of the laser beam. While light-induced thermal and chemical reaction-driven microswimmers can overcome this limitation, they generally operate in specific solution environments and are complex to fabricate, making large-scale production difficult. Therefore, developing light-driven intelligent microswimmers that can move freely under planar wave illumination, are not constrained by specific environments, and are suitable for large-scale manufacturing remains a significant challenge.

2.4 Microswimmer driven by light metamaterials

To address the limitation of optical force driven microswimmers that require highly focused lasers and exhibit movement trajectories dependent on light spot position [175,176], recent developments have integrated microfabricated nanophotonic structures into microswimmers [179, 71, 180]. This integration allows them to operate under plane waves or weakly focused light spots. In here, the discussion about these microswimmers are primarily focuses on the linear motion of microswimmers rather than the one only perform rotation. While numerous studies have reported the use of birefringence-based polarization conversion, as well as the transfer of spin [181–183] or orbital angular momentum [184–186] of light through absorption and scattering, to induce rotation in microparticles.

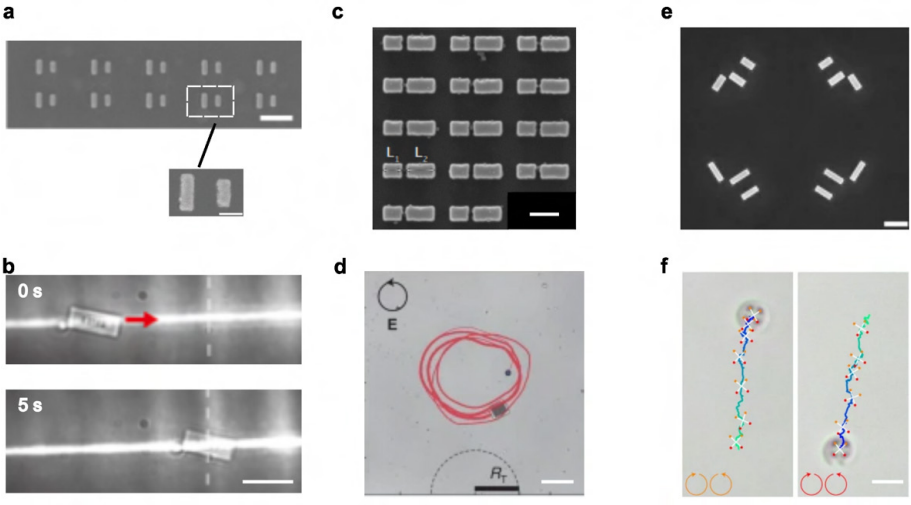

Figure 2.5: Microswimmer driven by nanophotonic structures. **a** Scanning electron microscopy (SEM) image of gold nanorod arrays designed to scatter light directionally. These nanorods are embedded in the microswimmer, allowing for linear movement when exposed to linearly polarized light, as illustrated in the bright field images shown in **b** [179]. Scale bars in **a** and **b** are 400 nm and 5 µm, respectively. **c** SEM image of silicon asymmetric dimer arrays engineered to maximize the efficiency of diffraction orders to +1. These arrays are embedded in a microswimmer that enables rotational movement along circular trajectories when subjected to circularly polarized light [71], as demonstrated in the bright field images shown in **d**. Scale bars in **c** and **d** are 400 nm and 20 µm, respectively. **e** SEM image of gold nanorods that selectively respond to circularly polarized light of specific wavelengths and handedness. These nanorods are embedded in a microswimmer, allowing for forward and backward movement by adjusting the circular polarization of two different wavelengths of light [180], as demonstrated in the bright field images shown in **f**. Scale bars in **e** and **f** are 200 nm and 2 µm, respectively. Images (**a**-**f**) are reproduced with permission from Refs. [179, 71, 180].

In 2020, Tanaka [179] et al. used electron-beam lithography (EBL) to fabricate gold nanorods with designed structures that exhibited asymmetric scattering under linearly polarized light. This asymmetry arose from detuned dipoles with different resonance frequencies oscillating with a phase difference, $\Delta\Phi$. When two dipoles are separated by a distance d, the scattered light experiences a phase delay of kd during propagation, compensating for $\Delta\Phi$ in one direction and reinforcing it in the opposite direction. By carefully designing the phase difference $\Delta\Phi$ and separation d, constructive interference (enhanced light) occurs in one direction, while destructive interference (diminished light) occurs in the opposite direction, leading to directional side-scattering. The gold nanorods (Fig. 2.5a) were embedded in rectangular SiO_2 microswimmers. The highly efficient asymmetric scattering generated a transverse optical force that propelled the microswimmers. In the optical focal line, generated by linearly polarized light and a cylindrical lens, the rotational Brownian motion of the microswimmers was suppressed, causing them to move in a fixed direction along the focal line ((Fig. 2.5b). When the polarization was perpendicular to the focal line, the motion ceased. By placing nanorods in four sections of the microblock with a 90-degree stepwise rotation, the microswimmers were able to rotate. However, due to the strong light absorption by the metallic structures [187], significant energy loss occurred, requiring higher light intensity to drive the system. Furthermore, gold deposited through sputtering often exhibited lower quality, reducing the efficiency of light manipulation.

Subsequently, Andren et al. [71] fabricated a metasurface using dielectric materials, specifically silicon, with each unit consisting of an asymmetric dimer structure (Fig.2.5c) embedded in SiO_2 microswimmers. These silicon nanostructures mimic a blazed grating but are constructed using two-dimensional fabrication techniques to enhance diffraction efficiency, concentrating most of the diffracted light in the $+1$ order while minimizing the 0 and -1 orders. This creates a transverse optical force that propels the microswimmers forward. The structure is polarization-sensitive: asymmetric diffraction occurs only when the light's polarization is aligned with the dimer's long axis, while the short axis shows no such effect. When the long axis is misaligned with the polarization, a restoring torque aligns the particle to the input light's polarization, enabling propulsion. Compared to previous work, the use of circularly polarized light introduces angular momentum transfer, causing the particle to rotate. The direction of rotation is determined by the polarization of the light. Due to the transverse force, the particle follows a circular path with a fixed radius (Fig. 2.5d). However, this design only allowed for forward motion and did not enable backward or lateral movement. To address this limitation, Wu et al. [180] improved the system by introducing two laser beams and designing structures that respond to specific laser wavelengths. By adjusting the size, structure, and distance between gold nanorods, they enabled the nanorods to selectively respond to circularly polarized light of a particular wavelength and handedness, generating directional scattering that creates torque to drive the microswimmers made from HSQ resist. Positioning nanorods with different wavelength responses in separate regions (Fig.2.5e) of the microparticle allowed two lasers and quarter-wave plates to control the handedness of circularly polarized light, enabling forward, backward, left, and right movement, as well as left and right rotation (Fig. 2.5f). Unlike previous designs that produced circular rotation with a radius, this setup enabled fixed-axis rotation. High-quality nanorods were achieved by transferring chemically synthesized single-crystal gold onto the surface for fabrication.

The fabrication of fast-moving microswimmers based on gold scattering structures

requires high-quality gold, which are obtained through chemical synthesis and transfer methods [188] that are incompatible with traditional microfabrication techniques. Additionally, gold's absorption of light results in lower efficiency. Therefore, in **Paper II**, I primarily focused on extending the silicon nanostructures discussed in the work of Andren et al. [71] to create microswimmers with complex movement trajectories.

2.5 Micromotors

The development of micromotors has paralleled that of microswimmers. As defined here, microswimmers primarily engage in swimming behaviors in solution, such as linear motion and rotation, while micromotors are predominantly characterized by rotational motion. In the development of human society, motors have consistently played a crucial role. From the earliest fluid-driven rotary motors, such as windmills and waterwheels, to steam-powered engines and modern electric motors, technological advancements in motor systems have continuously driven improvements in productivity. Whether in ancient handicraft industries or in today's highly industrialized society, motors have been fundamental to enhancing efficiency and advancing the industrialization process, making significant contributions to the progress of human civilization. Fifty years of development of Moore's Law has driven advancements in micro- and nanoscale fabrication technologies [189]. Over the past thirty years, research on motors has primarily focused on miniaturization, particularly at scales below 100 µm [190]. The miniaturization of motors offer numerous advantages, such as energy consumption, while large-scale manufacturing ensure cost reduction.

In 1989, Richard Muller et.al reported the fabrication of an electrostatically driven independent rotating micromotor using semiconductor microfabrication techniques [191]. This breakthrough attracted significant attention at the time, demonstrating the potential of silicon microfabrication methods for producing miniature movable components compatible with integrated circuits. It also highlighted the feasibility of creating microscale systems, inspiring continued efforts to develop increasingly smaller and more advanced microstructures [192–195]. In the process of motor miniaturization, the driving mechanism is one of the most critical factors determining the minimum achievable size of the motor. In addition to electrostatically driven motors [191,196–198], magnetic fields [199–203], AC electric fields [120, 204–206], and optical fields [182, 207, 208] are also employed to drive these miniature motors, with principles similar to those described in the previous section. However, a significant issue has been overlooked: most works have been focused on the development of individual micromotors, while the development of machine systems, particularly gear mechanical systems, has been neglected. Integrating individual motors into complex mechanical systems to drive them and achieve functional complexity is normal in macroscopic mechanical systems, such as those found in modern automotive, aerospace, and robotics applications [209]. The miniaturization of geared mechanical systems faces two primary challenges: motor-driven actuation and the coupling between different gears.

Traditional microfabrication techniques like conventional lithography enable precise alignment systems that facilitate gear coupling and meet commercial fabrication requirements. However, as shown in Fig. 2.6a, they require the fabrication of electrode or mechanical structures adjacent to the gears for actuation [210, 212]. When considering the space occupied by the driving system on the chip, the size exceeds 100 µm. This presents

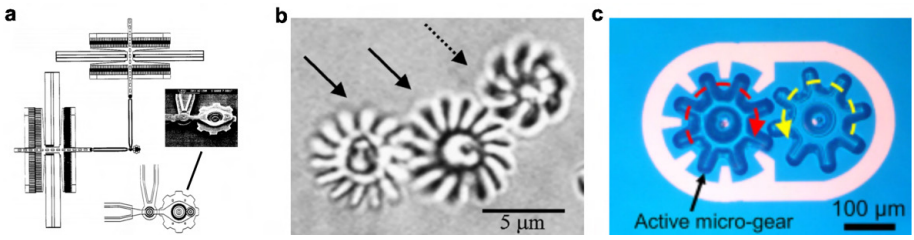

Figure 2.6: Microscopic geared mechanism powered by diverse approaches. **a** A conventional microfabricated electrostatic comb-driven microgear system featuring a single gear with a diameter of approximately 50 µm. The inclusion of a pin joint is necessary to connect the gear to the drive system, resulting in an overall system size exceeding 100 µm [210]. **b** An optical force-driven gear system featuring gears with three-dimensional structure. The coupling between the gears is facilitated by optical tweezers [211]. **c** A gear system driven by optoelectronic tweezers, where the rotation and coupling of the gears are facilitated by the electric field generated by the light pattern (indicated by the white area) [73]. In **b** and **c**, the gears decoupled in the absence of illumination. Images (**a**-**c**) are reproduced with permission from Refs. [210, 211, 73].

significant challenges, particularly when parallel control f multiple gear systems is required. While far-fields approaches such as magnetic, electric, light can address the challenge of space consumption by the the driving system, previously reported micromotors are normally incompatible with standard semiconductor fabrication processes, hindering the effective coupling between different gears. Magnetic [199–203] and AC electric field-driven [120, 204–206] motors require specific responsive materials, such as Fe_2O_3 or metals, which complicates the heterogeneous integration necessary for constructing multi-machine systems. In these systems, certain gears are required to respond to external fields, while other components must remain non-responsive to ensure proper functionality. Moreover, magnetic and electric fields provide synchronized control for all on-chip devices, making it challenging to achieve independent control of individual systems and thereby limiting their functional diversity. Optically driven motors are predominantly fabricated using polymers, such as photoresists, through two-photon lithography, resulting in complex three-dimensional (3D) structures [208]. This complexity necessitates multi-dimensional alignment, which poses significant challenges. Although some approaches use optical tweezers (Fig. 2.6b) [211] or optoelectronic tweezers (Fig. 2.6c) [73] for coupling, these methods are not integrated on the chip, as they tend to decouple and become unstable once the optical field is removed. Additionally, optical-driven motors normally rely on focused laser beams for control [182, 207, 208], presenting challenges for large-scale control. As demonstrated in the previous section, metamaterials address this issue. Metamaterials can be fabricated using tradition semiconductor techniques and are capable of movement under planar Wave illumination. In **Paper III**, metamaterials are introduced into the actuation of various gear mechanical system configurations, with fabrication achieved through standard photolithography processes.

2.6 Light-driven micromotors for fluid control

The control of fluids has been one of the fundamental area of research for centuries, from ancient waterwheels used to drive machinery to modern applications of fluid dynamics in power generation. Advances in this field have significantly contributed to technological progress and profoundly influenced human production systems and daily life. Fluid dynamics has played a key role in the development of agriculture, industry, and transportation throughout history. Current advances focus on the control of micro- and nanofluidics, enabling high-precision manipulation of fluids in extremely small volumes. This advance not only enhances our understanding of microscale fluid dynamics but also supports application in microfluidic chip technology, with great potential in drug screening, delivery, chemical reaction, and environmental monitoring. For instance, microfluidic chips facilitate efficient pathogen detection and biomarker anslysis for rapid diagnostics [74, 75]. They are also used in high-throughput chemical synthesis to accelerate reaction screeening, minimizing reagent and sample use while saving time [76, 76]. One of long-term objective in this field is to develop fully integrated automated liquid handling systems. This includes replacing large fluid control technologies like pressure-driven systems and syringe pumps [77–79], along with external analytical devices, to enable all fluid handling and analysis processes to occur on a single chip.

To address this challenge, many efforts have been made to enhance fluid manipulation techniques. This primarily involves utilizing physical gradients to control fluids through magnetic [111], electric, optical [215] and thermal fields. For example, in magnetic control, magnetic particles are introduced into the liquid and their movement is precisely adjusted using an external magnetic field [216]. This approach allows for accurate fluid manipulation without relying on traditional mechanical pumps or valves. Additionally, electric and optical fields can control fluid dynamics by inducing localized changes in pressure, temperature, or surface tension. These techniques are essential for advancing microfluidic chip technologies and other applications that require precise non-invasive fluid handling. Among these methods, light-driven techniques offer distinct advantages due to their lower material requirements. They don't require the introduction of charge or magnetic substances and can achieve more precise and parallel manipulation using focused light beam and light-modulated setups [217, 218].

Long range fluid manipulation using light can be categorized into few methods. One promising approach involves using light to generate heat that drives the flow, such as laser heating of water to create buoyancy-driven circular convection for transporting objects and concentrating particles ((Fig. 2.7a) [219]. Local thermal gradients can also be induced by nanostructures or nanoparticles that absorb light, thereby driving fluid flow. For example, as shown in Fig. 2.7b embedding chemically synthesized gold nanorods with dimensions on the order of tens of nanometers onto a glass substrate can induce an increase in temperature through the plasmonic resonance effect of the gold nanoparticles, thereby creating a thermal gradient that generates flow [214]. However, the unavoidable introduction of temperature changes, even when kept at lower levels, may still impact temperature-sensitive systems. The other approach involves generating electric fields through light to drive objects, such as using LED that employs digital micrometre devices (DMD) to create light pattern on the silicon substrate for controlling the rotation of gears and manipulating flow fields (Fig. 2.7d), However, this method operated at the scale of hundreds of micrometers,

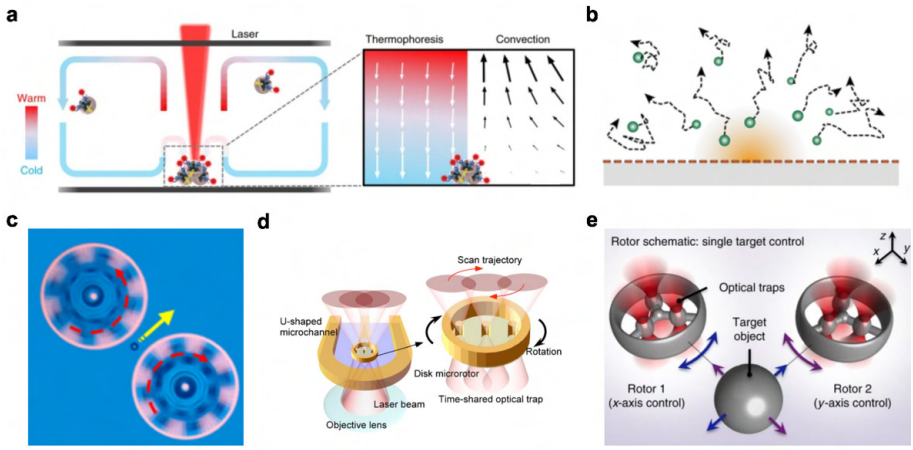

Figure 2.7: Fluid Manipulation through optical approaches a Schematic illustrating the accumulation of extracellular vesicles resulting from the interplay between thermophoresis and convection induced by localized laser heating [213]. **b** Schematic illustrating the dynamics of fluid flow in response to a localized temperature gradient generated by the light-induced absorption of gold nanoparticles on a substrate [214]. **c** Schematic illustrating the motion of a polystyrene microbead induced by fluidic flow generated by two microgears, which are driven by optoelectronic tweezers rotating in opposite directions [73]. **d** Schematic representation of a single-disk viscous micropump utilizing time-sharing optical forces to induce fluid motion [80]. **e** Schematic representation of the light field generated by the spatial light modulator, which drives the target object by rotating the rotor of the three-dimensional structure in varying directions to induce fluidic flow [81]. Images (**a**-**e**) are reproduced with permission from Refs. [73, 213, 214, 80, 81]

making it challenging to further reduce the size [73]. Additionally, it is limited to solution systems because high electrolyte concentrations can negatively impact manipulation efficiency. A different strategy draws inspiration from the structure of traditional mechanical pumps by utilizing the principle of optical tweezers to drive miniature mechanical components such as motors for fluid control. This method mitigates thermal effects and allows for better integration onto chips. For instance, as shown in Fig. 2.7d, light can drive a single on-chip motor to generate circular fluid flow, creating a valve-like effect [80]. Nevertheless, it often requires tightly focused lasers, which limits scalability. Despite the potential to use structured light devices, such as spatial light modulators (SLM), to control multiple mechanical components and manipulate fluids for micro-scale objects(Fig. 2.7e), this introduces significant complexity into the system. Since this method relies on feedback control [81], manipulating one rotor requires consideration of the flow fields generated by other rotating rotors, making it challenging to control movement, especially when generating more intricate flow fields. As demonstrated in **Paper III**, As demonstrated in **Paper III**, microfabrication techniques enable the large-scale fabrication of planar light-driven

motors, allowing for unrestricted motor configuration, adjustable rotation directions, and precise control over the distance between motors. Based on this, **Paper IV** show that the integration of motors that rotate clockwise and counterclockwise on the chip, generating arbitrary fluid fields through their rotation.

Chapter 3

Methodology

The topic of **Papers I-IV** is the innovation application of traditional micro- and nanofabrication techniques to the manipulation of micro- and nanoscale objects, specifically in the construction of new types of microswimmers, the fabrication of on-chip machines, and their application in microfluidic control. Over several decades, micro- and nanofabrication technologies have developed a comprehensive toolbox, including methods such as material deposition, lithography, and etching, which serve as essential technical foundatin for my research. In this chapter, I will briefly introduce the micro- and nanofabrication methods employed, as well as the key instruments used and their principles. Since the objects in this research are at the micro-scale, high-resolution digital video microscopy is essential for observation and measurement. Additionally, effective manipulation of these objects necessitates precise temperature control (**Paper I**) and the integration of an optical system with lasers (**Papers II-IV**) coupled to the microscopy. Therefore, the following section, which comes after the discussion of micro- and nanofabrication, provides a detailed description of the home-built experimental instruments. These instruments were specifically designed to enable precise and efficient control over micro- and nanoscale objects to support the research.

3.1 Micro- and nanofabrication

The chips or microparticles discussed in the thesis are at the micro and nano scale, necessitating the use of semiconductor chip manufacturing processes such as material deposition, photolithography, etching, and other tools [220, 221]. These processes are primarily divided into two categories based on the manufacturing methods: additive manufacturing and subtractive manufacturing.

Subtractive manufacturing involves directly processing and forming patterns from the original or deposited material, as illustrated in Fig. 3.1a. In this approach, a mask is created through photolithography, and the material is subsequently etched using physical or chemical methods to achieve the desired structure. This approach was primarily utilized in **Paper I** for the fabrication of disk-shaped particles, as well as for the creation of microwimmers in **Paper II** and micromachines in **Papers III-IV** on the chip.

Conversely, additive manufacturing constructs structures by introducing additional materials. The additive manufacturing method involves using photoresist to form a fixed

pattern, followed by material deposition and the subsequent removal of the photoresist to create the structure, which is called lift-off, as shown in Fig. 3.1b. The approach was used in **Paper I** for pattern substrate fabrictaion.

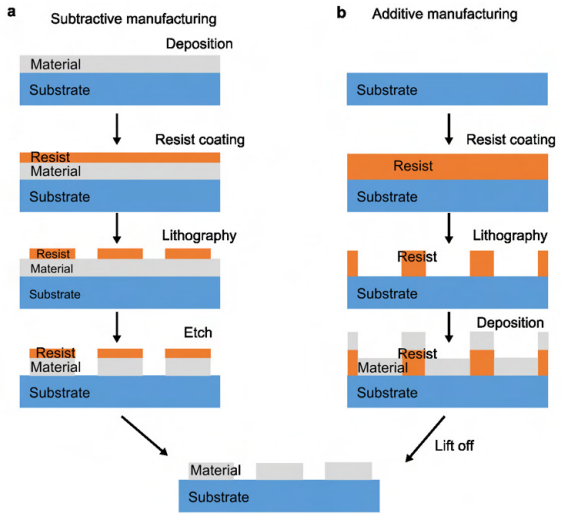

Figure 3.1: Overview of the two categories used for fabricating micro- and nanostructures. a Subtractive manufacturing process: This process starts with material deposition, followed by spin coating with resist. Lithography is then used to define the pattern on the resist, which serves as mask for subsequent etching to remove parts of the material, forming the micro- and nanostructure. **b** Additive manufacturing process (lift off): Similar to the process shown in **(a)**, the resist is used to define the pattern. However, in this method, material is deposited after the pattern has been defined. The final step involves removing the resist along with the unwanted material, leaving behind the desired micro- and nanostructure. This process is known as lift-off. Through **(a)** and **(b)**, micro- and nanostructure are formed on the substrate.

3.1.1 Matrial deposition

As illustrated in Fig. 3.1, material deposition is the initial step in the subtractive process and the concluding step in the additive process within micro-fabrication. The primary techniques for material deposition include chemical vapor deposition (CVD), physical vapor deposition (PVD), atomic layer deposition (ALD), and molecular beam epitaxy (MBE). My works predominately employs Chemical vapor deposition and physical vapor deposition.

Chemical vapor deposition (CVD) (Fig. 3.2a) operates on the principle of introducing volatile precursors into a reaction chamber, where they decompose or react on the heated substrate surface to form a thin film. The substrate is maintained at an elevated temper-

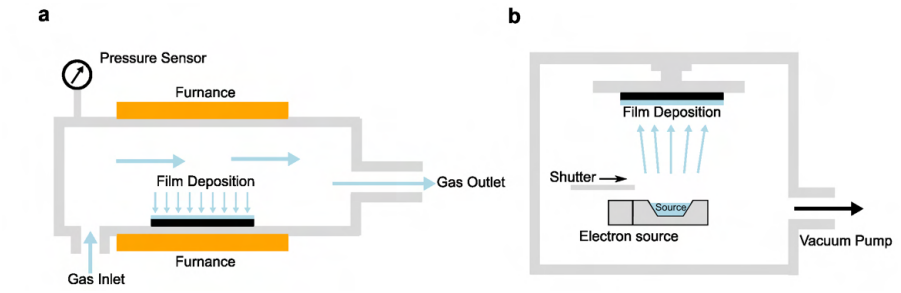

Figure 3.2: Overview of film deposition techniques. **a** Schematic diagram of a chemical vapor deposition (CVD) system, illusrating its main components:gas inlet, gas outlet, reaction chamber, pressure control unit, and furnace heating unit. The reaction precursor gas reacts on the substrate, which is maintained at a high temperature, resulting in the formation of a uniform film. **b** Schematic diagram of physical vapor deposition (PVD) via electron beam evaporation, depicting the primary components: electron source, vacuum pump, solid target source, and shutter. The process involves the use of high-energy electron beam to directly heat and evaporate the source material. The resulting vapor then condenses onto the substrate, forming a thin film.

ature to facilitate the chemical reactions, ensuring that the desired material adheres uniformly to the surface. CVD provides precise control over the deposition process, enabling the formation of uniform and high-quality films essential for semiconductor, insulator, and various functional layers in microelectronic devices. The process can be fine-tuned by adjusting parameters such as temperature, pressure, and precursor concentration, enabling the deposition of a wide range of materials with precise properties. Low-pressure CVD (LPCVD) and plasma-enhanced CVD (PECVD) are two common variants; LPCVD is performed at reduced pressures to improve film uniformity; for example, in **Papers II-IV**, high quality amorphous silicon was deposited using LPCVD. In contrast, PECVD utilizes plasma to enhance reaction rates and enable deposition at lower temperature; the SiO_2 in **Papers II-IV** was deposited using PECVD.

Physical vapor depoition (PVD) (Fig. 3.2a) involves the deposition of vaporized material directly onto the substrate through condensation. PVD techniques, including sputtering and evaporation, operate without chemical reactions; rather, they utilize the physical transport of atoms or molecules from a source to the substrate. This method is particularly effective for depositing metal and alloy films that exhibit high purity and strong adhesion. PVD processes are versatile, capable of being executed under various pressures and temperatures, which allows for the tailoring of material properties and film characteristics to specific requirements. However, PVD may have limitations in achieving uniform coatings on complex geometries and may not offer the same level of precise control over film composition as CVD. In **Paper I**, the PVD was used to deposit the titanium/gold layer on glass substrate.

3.1.2 Lithography

Micro- and nanostructures are defined using resist materials, which are polymer-based substances that can be patterned through various lithographic techniques. Among the commonly employed lithography methods are electron beam lithography (EBL), photolithography, and nanoimprint lithography. This thesis utilizes EBL and photolithography.

Electron beam lithography employs a finely focused beam of electrons to create precise patterns on a resist-coated substrate. The interaction of the electron beam with the resist induces localized chemical changes, allowing for the formation of intricate and high-resolution patterns at the nanoscale. This technique is particularly suited for applications requiring exceptional patterning accuracy and complexity.

A key feature of EBL is the use of magnetic lenses to precisely control and focus the electron beam. These lenses direct the electron paths, enabling the creation of fine features without the need for physical masks. This maskless approach offers significant flexibility in pattern design, as the electron beam directly defines the pattern, allowing for the rapid adjustment of pattern sizes and shapes.

The exceptional resolution of electron beam lithography is largely attributed to the Small wavelength of electrons compared to visible light. Electrons, when accelerated to high energies, have wavelengths on the order of picometers, which are much smaller than those of visible light. This smaller wavelength enables the electron beam to resolve features at the atomic scale, making the technique particularly advantageous for applications in advanced semiconductor devices, nanotechnology, and high-performance optical components. The patterned substrate in **Paper I** and metasurface in **Paper II-IV** were defined by EBL.

In contrast to EBL, photolithography utilizes the interaction between photons and photoresist to define patterns. In modern semiconductor manufacturing, photolithography employs various light sources-from ultraviolet (UV) to deep ultraviolet (DUV) and even extreme ultraviolet (EUV)-with patterning accuracy determined by the wavelength of light. Conventional photolithography requires masks, through which light passes to project the pre-defined pattern onto the photoresist. This method is efficient and cost-effective for high-speed, high-volume production.

However, in scientific research, where frequent design revisions are necessary, fabricating new masks for each iteration can be both time-consuming and labor-insensitive. To overcome this limitation, maskless photolithography techniques are employed. These methods, including direct laser writing using tools such as digital micromirror devices (DMD) and spatial light modulators (SLM), avoid the need for physical masks. They use programmable optics to dynamically control the light's propagation path, directly exposing the photoresist to form the desired pattern. In direct laser writing, a focused laser beam scans across the photoresist, varing the light intensity or exposure time to precisely alter the properties of photoresists. This technique offers significant flexibility and precision, facilitating rapid pattern adjustments and efficient fabrication of complex micro- and nanostructures. In my research, direct laser writing is predominantly used to define micrometer-scale patterns, as detailed in **Papers I-IV**.

3.1.3 Etching

In the subtracting manufacturing process, after the pattern is defined through photolithography, the material is subjected to etching. Chemical etching involves a reaction between the material and a reactive gas or solution to remove it. Conversely, physical etching used ion bombardment to dislodge and remove material from the substrate. This thesis predominantly employs reactive ion etching (RIE), which integrates both chemical and physical etching mechanisms. RIE operates by generating a plasma of reactive ions in a vacuum chamber, which then interact with the material's surface. The chemical reactions between the reactive ions and the material lead to its removal (Fig. 3.3a), while the physical impact of the ions assists in the etching process. RIE provides enhanced etching selectivity and anisotropy, making it ideal for creating well-defined micro- and nanostructures. Halogens, such as fluorine and chlorine, are commonly used as reactive gases in RIE due to their high reactivity and ability to form volatile compounds with various materials. This ensures efficient and precise etching of materials like Si, SiO_2, Si_3N_4, contributing to the overall effectiveness of the etching process.

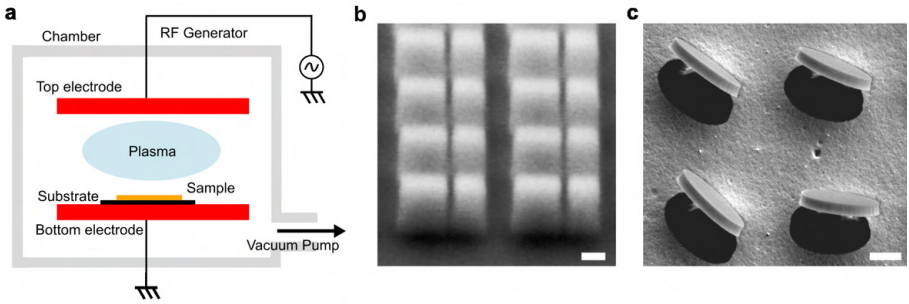

Figure 3.3: Overview of etching techniques. a Schematic diagram of a reactive ion etching (RIE) system. The upper and lower electrodes, typically powered by RF energy, generate and sustain low-pressure plasma. RF power applied to the electrodes accelerates ions through the electric field, causing them to bombard the material surface with high energy. This bombardment induces chemical reactions, thereby increasing material removal rates and achieving finer etching precision. **b** Scanning electron microscopy images of silicon metastructures in **Paper II-IV**. The anisotropic etching results in straight pillars. Scale bar: 200 nm. **c** Scanning electron microscopy images of microdisks in **Paper I**. The isotropic etching lifts the microdisks out of the substrate. Scale bar: 1 µm.

The etching can be divided into anisotropic and isotropic etching. Anisotropic etching removes material predominantly in one direction, typically vertical, resulting well-defined straight sidewalls. This type of etching is crucial for applications requiring high aspect ratio structures with precise geometries. Anisotropic etching can be achieved by controlling the radio frequency (RF) bias in process like RIE. By adjusting the RF bias, the energy and directionality of the ion bombardment can be controlled, enhancing vertical etcing and reducing lateral etching. This ensures that the etching primarily occurs in the vertical

direction, achieving the desired anistropic. For example, in **Papser II-IV**, the a-silicon metastructure is achieved by the anistropic etching through the cl2 gas (Fig. 3.3b).

Isotropic etching, in contrast, removes material uniformly in all directions, leading to rounded or undercut features beneath the resist mask. This type of ecthing is often used when precise control of vertical sidewalls in not critical. The uniform removal of material in isotropic etching can be advantageous for application where smooth, curved sufaces are desired. Isotropic etching can be controlled by adjusting parameters such as gas composition, pressure, and RF power to ensure that the etching occurs evenly in all directions. In micro electron mechanical systems (MEMS) field, isotropic etching is frequently employed to release sacrificial layers, facilitating the creation of free-standing structures. For example, the microparticles or micromachines in **Papers I-IV** are released by isotropic etching of silicon under the SiO_2 using SF6 gas, as the etching rate of Si is much faster than that of SiO_2 with SF6 (Fig. 3.3c).

3.2 Measurement

The research presented in **Paper I-IV** focuses on the micrometer scale, with precise control achieved through temperature regulation and optical methods. This requires the construction of specialized measurement setups, including a microscope and systems to apply external fields such as light and heat. The primary setups developed for my research include a temperature control system, used in **Paper I**, and a laser control system, utilized in **Paper II-IV**.

3.2.1 Temperature control setup

The home-built setup used in **paper I** is divided into two parts, the temperature control of the sample and optical microscopy. As illustrated in Fig. 3.4. To track the movement of the particles, standard digital video microscopy with white light illumination and a CMOS camera is employed. This method allowed for high-resolution imaging and precise tracking of particle dynamics in real-time.

Achieving and maintaining precise temperature control of the sample is crucial for the experiment and is carried out in two sages, as detailed in reported studies. Initially, the sample temperature is stabilized at 32.5 °C using a circulating water bath (Model T100, Grant Instruments) connected to the stage below the sample. This setup ensured that the temperature is kept well below the critical temperature $T_c \approx 310\,\mathrm{K} \approx 34\,^{\circ}\mathrm{C}$, minimizing any unintended thermal effects that might affect the subsequent more sophisticated temperature control.

In the second stage, a more refined temperature regulation is achieved using a feedback control system. This system includes a peltier heating/cooling element and a PT 100 temperature sensor. The Peltier element is connected to the 100× oil objective, controlling the temperature of the oil and thus the sample by heating the objective. The feedback controller allows for precise adjustments, maintaining the sample temperature with a remarkable stability of $\pm 20\,\mathrm{mK}$. This two-stage temperature control mechanism ensures that the experimental conditions remain consistent and accurate throughout the observation, providing reliable and reproducible data for analysis.

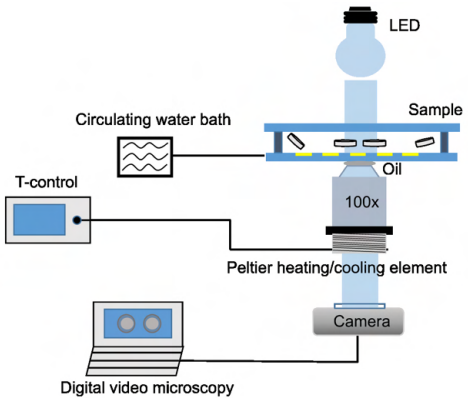

Figure 3.4: Experiment setup for temperature control. A schematic of the custom-built setup combining digital video microscopy and precise temperature regulation. The microscopy system features white LED illumination and a 100× objective, capturing scattered light and connected to a computer for video analysis. Temperature control involves two stages: a circulating water bath for coarse regulation (±100 mK) and a Peltier element on the oil-immersion objective for fine control (±10 mK), ensuring overall stability within ±20 mK.

By employing this technique, it is possible to monitor and analyze the motion of particles with high temporal and spatial resolution, enabling a detailed study of the underlying physical phenomena.

3.2.2 Optical control setup

In **Paper II-IV**, an home-built setup combining a laser and microscopy is used to control the movement of microswimmers and micromachines. As illustrated in Fig. 3.5, the optical setup is divided into two main components: a bright-field home-built optical microscope and an illumination system. The microscope is employed to observe the motion of microswimmers and micromachines, while a1064 nm laser is used to drive their movement.

For the setup details, a half-wave plate and a polarized beam splitter (PBS) are utilized to horizontally polarize the 1064 nm light. The half-wave plate also controls the power of the incident laser on the sample. The laser that passes through the PBS is then expanded in beam size by passing through two lenses, L1 and L2. These lenses are used to weakly focus the beam onto the sample, producing a spot diameter of 200um to ensure large-area control of the microswimmers.

A half-wave plate and quarter-wave plate are positioned in front of the sample to generate linearly polarized and circularly polarized light, respectively. Additionally, an LED light provides illumination from above the sample, while a 20× air objective below the sample generates a large field of view. The motion of the objects is recorded using a CCD camera, with an infrared filter in place to filter out the 1064 nm laser and prevent

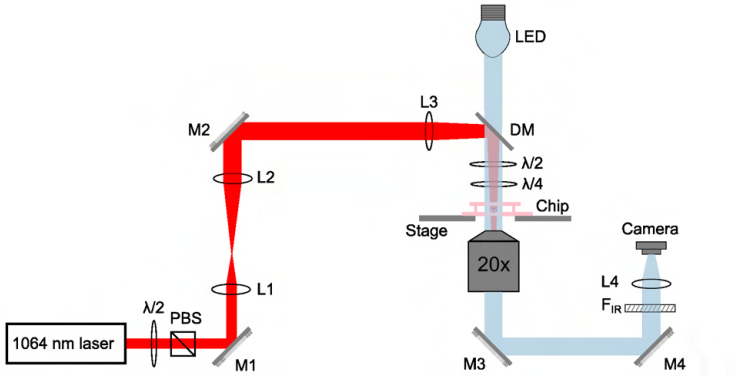

Figure 3.5: Optical setup. The 1064, nm continuous-wave laser beam is expanded to approximately 1, cm in diameter using a telescope system (L1, L2) and then focused through a lens (L3) to achieve a spot size of about 300, µm. The laser's output power is manually adjusted using a half-wave plate ($\lambda/2$) and a polarizing beam splitter (PBS). The polarization state is controlled with a combination of half-wave ($\lambda/2$) and quarter-wave ($\lambda/4$) plates after the dichroic mirror (DM), enabling either linear or circular polarization. The 20× objective and CMOS camera capture the movements, while an infrared filter blocks the 1064, nm light to protect the camera. PBS: Polarizing beam splitter; M: Mirror; L: Lens; DM: Dichroic mirror; F_{IR}: Infrared filter; $\lambda/2$: Half-wave plate; $\lambda/4$: Quarter-wave plate.

any potential damage to the camera.

Chapter 4

Research results

In this chapter, I present the results in four sections, each based on one of four distinct studies. The first section introduces periodic gold-SiO_2 structures fabricated through micro- and nanoscale techniques to investigate critical Casimir torque as an approach for achieving nanometer-scale precision in manipulating the movement of micron-sized passive particles. The second section transitions from passive particles to active microswimmers, achieved by embedding optical nanostructures within the particles. This approach enables the particles to harness energy from laser irradiation, leading to deliberately designed complex motion. The third section details the integration of these particles onto a chip, forming on-chip motors arranged in gear-like configurations to create sophisticated, functional micromachines capable of autonomous motion. Finally, the fourth section explores the application of these micromachines in fluidics control, demonstrating their ability to generate complex and controllable fluid flow patterns.

4.1 Nanoalignment by Critical Casimir Torque

As discussed in the background, manipulation of the movement of micro- and nanoparticles through temperature changes on a large scale remains challenging. the critical Casimir force generated by density fluctuations at the critical temperature in the binary liquid can be used to influence the movement of particles, such as trapping [222], bonding [148, 49], assembling [48]. However, experimental research employing the critical Casimir force, particularly critical Casimir torque, for advanced on-chip manipulation of microparticles with nanometer precision and more complex control remains limited, despite several related theoretical studies [223–225]. This motivated our research in **Paper I**.

In **Paper I**, critical Casimir force, both attractive and repulsive, along with electrostatic forces, were employed for particle manipulation. First step is to generate the critical Casimir attractive and repulsive force. Whether critical Casimir force is attractive or repulsive depends on the wet properties of substrate. Specifically, when two surfaces share same wettability (e.g., both hydrophilic or both hydrophobic), an attractive force arises. In contrast, when the surfaces exhibit opposing wettability, a repulsive force is observed. Here, SiO_2 was chose as the hydrophilic material due to the presence of surface hydroxyl groups, which confer a negative charge and hydrophilic properties. The hydrophobic surface was prepared by depositing a thin gold layer onto a glass substrate, followed by the

application of a thiol coating. The thiols were self-assemble on the gold surface through sulfur-gold bonds, with the opposite terminal group presenting hydrophobic properties. This self-assembled monolayer remains stable for up to two months under ambient conditions. To investigate the attractive and repulsive forces, microfabrication techniques were employed to fabricate a disk-shaped particle, When the SiO_2 disk particles were on the glass substrate, both hydrophilic, the close of temperature to the critical temperature (the temperature control setup is shown in methodology section) induced the critical Casimir attractive force. This caused the disk particles to approach the substrate, reducing particle diffusion due to the stronger hydrodynamic effect (Fig. 4.1a), which increases as the distance between the particles and substrate decreases. In contrast, the critical Casimir repulsive force dominates for particles on the gold surface, increasing the distance between the particles and the substrate, thereby enhancing diffusion, as illustrated in Fig. 4.1b.

I demonstrated that tuning the properties of the substrate can be used to induce either critical Casimir attractive or repulsive forces, which in turn modulate the motion of the disk particles. I employed microfabrication techniques to integrate two surfaces with distinct properties onto a single substrate. This process involved EBL, thin film deposition via Evaporation, and lift-off process (details of the techniques are shown in methodology section). Due to the gold the thickness of gold film is 25 nm, the entire substrate can be considered flat. The SiO_2 regions of the pattern generate an attractive force, while the adjacent gold regions produce a repulsive force. This combination created a harmonic potential that effectively traps the particles at the center of the pattern, as shown in Fig. 4.1c. The patterns are not limited to capturing disk particles; they can also trap colloidal particles. Compared to disk particles, colloidal particles have a smaller contact area with the substrate, leading to a reduced critical Casimir force. Since the critical Casimir force is positively correlated with surface area, the substrate exerts a weaker trapping potential on colloidal particles, resulting in increased diffusion relative to disk particles.

In the experiment, I found that changing the temperature causes disk particles to exhibit both parallel (Fig. 4.1c) and perpendicular (Fig. 4.1d) orientations relative to the substrate. These two configurations do not exist independently but coexist, each appearing with a certain probability. This probability can be controlled by adjusting the pattern size on the substrate and the temperature. According to the experiment results, my collaborators Pitor Nowakowski and Svyatrslav Kondrat conducted theoretical simulation, confirming that it is primarily driven by the balance between critical Casimir attractive and repulsive forces, as well as electrostatic force and gravity. When the pattern size exceeds the particle size, the particle is primarily influenced by the critical Casimir attractive force, with the repulsive force being negligible. This increase the probability that disk is oriented parallel to the pattern. Conversely, as the pattern area decrease, the critical Casimir repulsive force acting on the particle becomes greater than the attractive force, causing the particle to favor a perpendicular configuration. Based on this, we designed an oval-shaped pattern that encourages the disk particle to be perpendicular to the substrate. The orientation of the perpendicular configuration is determined by the orientation of the oval pattern on the substrate, unlike in circular patterns, where the particels are perpendicular to the surface but exhibit random orientations. Therefore, the particle aligns with the shape of the pattern to minimize trapping energy when it is on the patterned substrate. Based on this, I fabricated a chiral particles formed by the

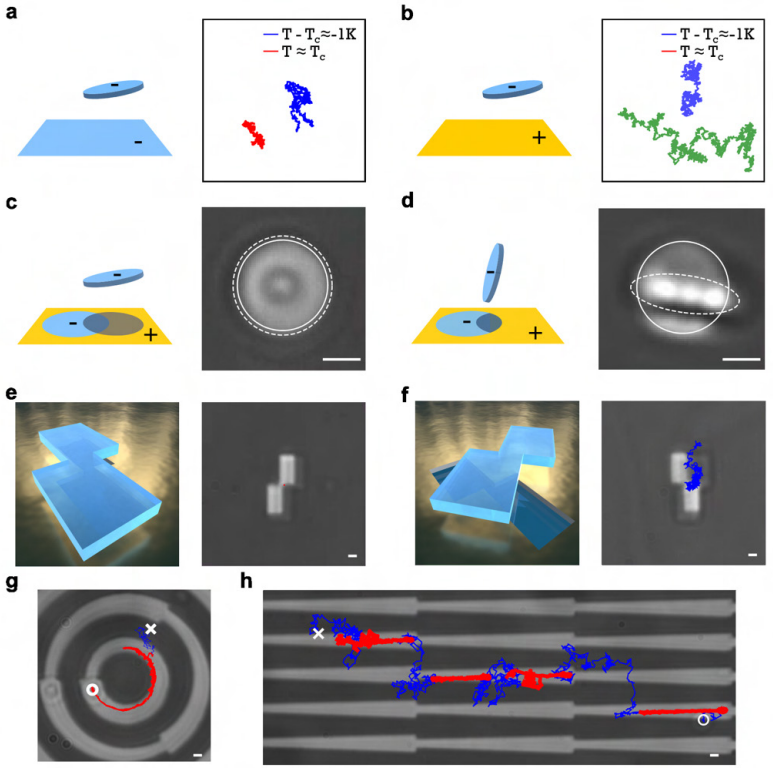

Figure 4.1: Particle manipulation using patterned substrates via critical Casimir force. Schematic and trajectories of a disk particle on **a** glass and **b** gold substrates near the critical temperature. The critical Casimir attractive force on the glass substrate reduces diffusion, while the repulsive force on the gold substrate enhances diffusion at the critical temperature. The symbols + and − represent hydrophobic and hydrophilic interactions, respectively. Schematic and optical microscopy images of trapped disk particles oriented **c** parallel and **d** perpendicular to the substrate around the critical temperature. The right chiral disk particles, composed of two rectangles, are trapped on a **e** right chiral pattern and diffuse freely on a **f** left chiral pattern around the critical temperature. **g** The disk particle moves along a long trajectory, with the red trajectory indicating linear movement along the triangle due to Brownian ratchet effects at the critical temperature, and the blue trajectory representing free diffusion. **h** Disk particle move with a circular trajectory on the curved triangle. In **g** and **g**, the cross and the circle indicate the trajectory starting and finishing points, respectively. Scale bars are all 10 µm. Images **c**-**h** reproduced with permission from Ref. [226].

misalignment of two rectangles. In the experiment, I observed that particles were trapped by patterns matching their chirality, as shown in Fig. 4.1e; if the chirality did not match, the particles remained unstable and eventually detached from the pattern (Fig. 4.1f). Left-handed particles aligned with left-handed patterns, while right-handed particles aligned with right-handed patterns.

Different pattern can be designed to create various potentials for manipulating particles, not just for trapping them. Thus, I aimed to design a pattern that make the particle move. Based on the relationship between critical Casimir force and the area of the pattern, I designed a triangular pattern. As the area from the tip to the base of the triangle increases, the applied critical Casimir repulsive force on the disk particles become greater than the attractive force, restricting the Brownian motion of particles toward the tip and causing them to move toward the base of triangle. By altering the length ratio of the base to the height of the triangle, the speed of the particle can be adjusted. The manipulation of particle movement is not limited to linear motion; the triangle can be bent to allow the particle to move in a circular trajectory (Fig. 4.1g). However, the distance the particle can move is limited. As the base of the triangle becomes smaller relative to the height, the difference between the critical Casimir repulsive and attractive forces on the triangle diminishes, hindering the particle's movement. To enable the particle to move in a long direction, I fabricated a series of superimposed triangles. By adjusting the temperature close to the critical temperature, the particle moves along the triangle and approaches the bottom. Then, by decreasing the temperature away from the critical temperature, the particles leave the pattern and move randomly off the triangle. Immediately afterward, increasing the temperature allows the particles to be trapped by the next triangle, continuing their movement along it. By repeating this process multiple times, the particles can move in a single direction for hundreds of microns or even longer, as shown in Fig. 4.1h.

In conclusion, **Paper I**, I demonstrated a method to manipulate micro-sized particles with high precision using the critical Casimir force. This method requires onlt temperature control and allows for parallel, large-scale manipulation of particles without special requirements regarding their properties. Specifically, the particles do not need to be magnetic, electrical, or transparent; they only need to be hydrophilic or hydrophobic. This process provides a platform for studying the physical and chemical properties of particles and for self-assembling functional materials, such as micro-LEDs and two-dimensional material disks.

Contributions to the work:

In Paper I, I have fabricated the particles and substrate in cleanroom at Chalmers University of Technology. I have designed and performed the experiments, analyzed the data and prepared manuscript and figures for publication. The theoretical model and simulations of this work have been done in collaboration with Pitor Nowakowski from Max Planck Institute for Intelligent Systems in Stuttgart.

4.2 Microswimmers driven by metasurface

Modest progress has been made in controlling micro- and nanoparticles in liquid by using external fields to conunter the effects of Brownian motion [27,28,85,30,86,29,87–89]. One promising development is the creation of self-propelled particles, called microswimmers, which gather energy from their surroundings to move on their own. These particles mimic biological systems, like bacteria, and offer insights into microbial movement and non-equilibrium dynamics [149, 150]. They hold potential for applications such as targeted drug delivery [61, 165] and environmental cleanup [227, 228]. While most current designs rely on a Janus structure, which limits their functionality, future research aims to develop more autonomous microswimmers with open-loop control for improved navigation and interaction. Optical control has gained prominence over electric and magnetic methods due to its precision in manipulating microswimmers through focused light [173]. While optical tweezers effectively control particles, they often require tightly focused light [174,176,175], limiting motion to feedback-controlled paths and necessitating illumination at multiple points for complex operations. Recent studies have explored the use of nanostructures to enhance light scattering and diffraction, allowing microswimmers to operate in plane wave or weakly focused light fields, thus enabling movement across larger areas [179, 71, 180] (more details in background section). By modulating light polarization with open-loop control, both linear and rotational motion can be achieved. However, current motion trajectories are primarily linear or circular. Future research should aim to optimize these systems to facilitate more complex movement patterns, such as elliptical trajectories and fixed-point rotations, thereby advancing the development of intelligent microswimmers.

To address this challenge, inspired by the work published by the Mikael Käll group [71], the microswimmer is fabricated using microfabrication techniques that combine material deposition, electron beam lithography (EBL), and reactive ion etching. Details of fabrication and the measurement setup for movement of microswimmer under illumination are presented in methodology section. I started by designing a silicon metasurface, which acts as a grating capable of efficiently diffracting incident light into the +1 order, enabling precise momentum transfer that drives the linear motion of microscopic particles, as shown in Fig. 4.2a. To achieve more complex movement trajectories, I divided the microswimmer into four parts, each covered by metasurfaces with different orientations. These metasurfaces convert incident light's momentum into forces in various directions but same magnitude. When forces direction on adjacent parts are 90° apart, they generate optical torque due to their directional differences, causing the microswimmer to rotate around its center (Fig. 4.2b). The Adjustment of the metasurface's orientation can controls the rotation direction of the microswimmer, allowing for either clockwise or counterclockwise rotation. Fine-tuning the torque further enables elliptical trajectories, with the profile and direction of trajectory controlled by adjusting the force magnitude. The movement of the microswimmer can also be controlled by selectively embedding the metasurface on certain regions. For example, when the metasurace was only embedded on half area of the microswimmer, the force applied became asymmetric, shifting away from the center of mass. This imbalance generated torque, causing the swimmer to rotate around its center, as shown in Fig. 4.2c. By tuning the force magnitude, the radius of the rotational trajectory can be adjusted, enabling diverse curved movement trajectories.

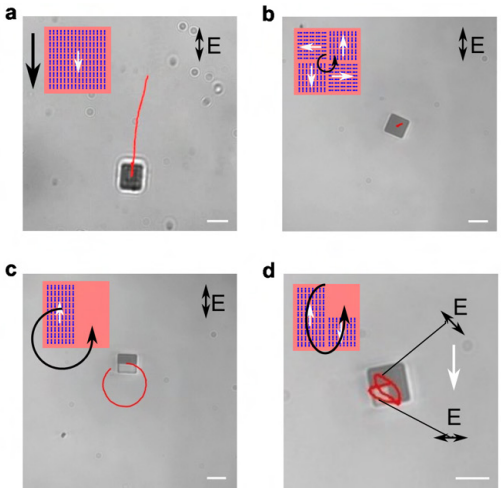

Figure 4.2: Light-driven microswimmers with metasurfaces-controlled behaviors. **a** The microscopy images show a microswimmer exhibiting linear motion under linear polarization, driven by the unidirectional arrangement of metasurfaces. This configuration generates a force in a single direction, propelling the microswimmer forward. The inset provides a schematic representation of the microswimmer, with blue sections depicting the metasurfaces. The white arrow indicates the generated force, while the black arrow shows the direction of the microswimmer's motion. The red line represents the microswimmer's trajectory. **b** The microswimmer rotates locally around a single point, with metasurfaces positioned in four distinct regions. The orientations of the metasurfaces are arranged progressively at 90-degree intervals in a counterclockwise direction, generating forces (white arrows) in four directions under linear polarization. These forces produce an optical torque, leading to the rotation of the particle in counterclockwise direction (black arrow). **c** The microswimmer, with metasurfaces located in only half of its structure, performs counterclockwise rotation with a radius under linear polarization. **d** The microswimmer exhibits an elliptical rotational trajectory under linear polarization. When the direction of linear polarization is altered, the elliptical motion trajectory also changes accordingly. In the microscopy image, the linear polarization is dynamically changed from 45° to vertical, resulting in a corresponding dynamic change in the trajectory. The scale bars in **a-d** are all 10 µm.

The propulsion of microswimmers originates from the metasurface, allowing their movement to be independent of specific shapes. The flexibility of traditional photolithography enables the fabrication of microswimmers in various geometries. Thus, in addition to controlling movement by adjutsing the metasurface design, further optimization of movement can be achieved by altering the geometric shape of the microswimmers, such as circular, square, or L-shaped configurations. The shape of the microswimmer significantly influences its motion primarily due to hydrodynamic effects. Hydrodynamic principles indicate that different geometries can alter the fluid flow field around the microswimmer,

affecting the forces acting on it and its trajectory.

As the metasurface is sensitive to the polarization of light, it enables dynamic control of the behavior of microswimmers through the adjustment of polarization state. For instance, a microswimmer exhibiting elliptical motion has its elliptical direction determined by the orientation of the linearly polarized light. Specifically, when the light is horizontally polarized, the major axis of the ellipse extends horizontally, while a vertically polarized light aligns the major axis vertically. Therefore, by dynamically altering the direction of the linearly polarized light, the elliptical trajectory of the microswimmer can change accordingly, creating elegant shapes reminiscent of flowers (Fig. 4.2d). This capability could have potential applications in environmental exploration.

In collaboration with Edoardo Manoni, we developed a theoretical model based on the Langevin equation to describe particle movement. The trajectories predicted by this model closely match the experimental results. In summary, in **Paper II** by adjusting the distribution of the metasurface on the particles and the geometric shapes of the microswimmers, I can design a variety of complex behaviors. This flexibility allows for the customization of movement trajectory and enhances adaptability across different application scenarios.

Contributions to the work:

In **Paper II**, I have designed the experiment and fabricated the microswimmers in the cleanroom at Chalmers University of Technology. I have performed measurement of their behavior and wrote the code to obtain the trajectories of the microswimmers. The theorretical model to simulate the behaior of the microswimmers have been developed by Edoardo Manoni and me.

4.3 Microscopic Geared Mechanisms

As discussed in background section, significant challenge persist in constructing on-chip micrmachine below 100 µm [190,191,73], The definition of a machine here refers to different components combined together to achieve a complex task.. This challenges arise from the need to balance large-scale manufacturing, precise coupling of various components into machines, and far-field driving methods while minimizing the spatial waste generated by traditional electrostatic micromachines [191], which require driving components around them. Metasurfaces, which can effectively address these issues, have emerged as a key solution.

In **Paper III**, the first step in building a mechanical system is constructing a motor. Using phase gradient metasurface to drive the motore requires solving two key challenges. The first is how to induce rotation. Following the approach in **Paper II**, I arranged four adjacent metasurfaces embedded in the motor at perpendicular orientations (Fig. 4.3a). This design ensures that the forces generated under linear polarized light illumination produce optical torque, causing the motor to rotate (Fig. 4.3b). The second challenge is integrating the motor on the chip. I designed the motor configuration using donut-shaped disk particles with silicon metasurfaces made of SiO_2 as rotors. SU8 pillar and cap are constructed in the center of the disk, serving as stators to restrict the disk's movement in both two-dimensional and three-dimensional directions. Here, I need to describe the fabrication process of the three-dimensional structure involving the pillar and cap, as this is a newly developed method compared to **Paper II**. After fabricating the disk, I spin-coat a 4 µm thick layer of SU8 photoresist, then expose and develop it to form a pillar inside the hole of the disk, as shown in Fig. 4.3c. The pillar is much higher than the disk, restricting the disk's rotation within a limited two-dimensional range and making any lateral movement difficult. Then, I spin-coat a layer of positive photoresist and reduce its thickness until it is slightly lower than the pillar. Another layer of SU8 photoresist is then spin-coated and exposed to form a cap, which connects to the pillar. Once the positive photoresist is removed with an organic solvent, the cap remains suspended above the disk particle without making contact, ensuring the particle's rotation is unaffected while limiting its movement in the three-dimensional direction (Fig. 4.3d). The pillar and cap securely fix the disk to the chip, preventing detachment even under significant environmental fluctuations.

Under illumination, the motor rotates continuously. Since it is driven solely by light and made of chemically stable materials, such as SiO_2 and SU8, it can operate for months or even years if properly packaged to prevent water evaporation. As the light intensity increase, the speed of motor also increases. Notably, I discovered that the relationship between motor speed and light intensity is not linear. My collaborator Mahdi Shanei and I propose that this is primarily due to the Si metasurface embedded in the motor absorbing light, which raises the surrounding temperature and reduces the viscosity of the liquid [229]. Mahdi Shanei used COMSOL to conduct photo-thermal simulation to validate this hypothesis, and the absorption coefficient of Si was measured using an Ellipsometer. In addition to light intensity, the rotation speed of the motor was adjusted by the number of asymmetric dimers that comprised the metasurface. A large number of dimers resulted in greater optical torque, which in turn increased the rotation speed. Because the motor was not limited to highly focused light for operation and was fabricated using conventional

photolithography process, different motors could be created on the same chip, regardless of their shapes and sizes, and could rotate simultaneously under illumination. The minimum motor size I was able to fabricate had a diameter of 8 µm. This limitation was due to two factors: first, the need to include enough metasurface elements to generate sufficient force to overcome the liquid's friction and enable rotation; second, the constraints of the fabrication process itself, though with optimization, even smaller motors could potentially be achieved.

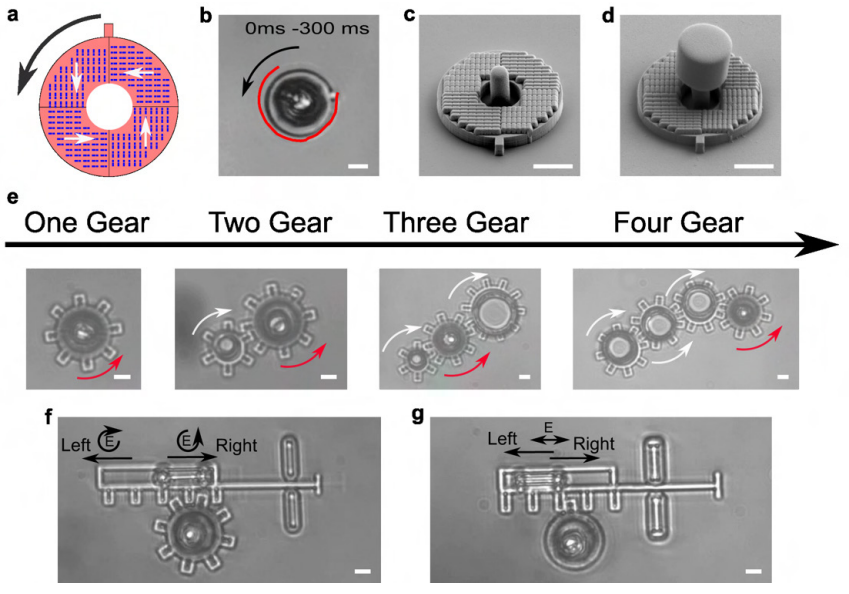

Figure 4.3: Light-driven micromachines. **a** Schematic of a micromotor embedded in metasurfaces. The blue metasurface is divided into four sections, generating forces (white arrows) in four directions to produce optical torque, driving counterclockwise (black arrow) rotation of the micromotor. **b** Optical microscopy images showing the counterclockwise rotation of the micromotor. Micromotor integrated on a chip using the **c** pillar and **d** cap to limit movement in three dimensions. **e** Optical microscopy images of gear systems with varying numbers of gears, where active gears (with metasurfaces) drive passive gears (without metasurfaces). Red arrows indicate the rotation direction of the active gears, while white arrows show the rotation direction of the passive gears. **f** Optical microscopy images of a gear and rack system. The rotation of the gear induces left and right linear movement of the rack by changing the circular polarization to counterclockwise and clockwise. **g** Optical microscopy images of a single-tooth gear and rack system. The rack moves left when the gear touches it and moves right without contact, as the metasurface on the rack generates a force to push it under linear polarization. All scale bars: 5 µm.

With the motor available, the next step is to utilize it to drive complex machine systems. Using traditional microfabrication processes that achieve nanometer-scale align-

ment accuracy for overlay, other mechanical components built around the motor can be successfully coupled to it. The coupling between components was achieved using gear configurations (Fig. 4.3e) commonly found in macroscopic mechanical systems. I fabricated a series of two gears, with a driving gear controlling the rotating of passive gears of varying sizes. The difference between the driving gear and the passive gears was the presence of the embedded metasurface. The fabrication process was determined by whether the metasurface was defined in the Silicon during the first fabrication step, while the subsequent fabrication steps remained the same for both gears. The angular velocity ratio between the driving and passive gears corresponded to the ratio of their diameters. This meant that the angular velocity of the passive gear could be adjusted based on the angular velocity of the driving gear and their relative diameters, a concept known as mechanical advantage in gear systems. By modifying the size of the gears, both the torque and speed of the system's output were controlled. The purpose of this experiment was to demonstrate that macroscopic gear systems can be scaled down to less than 100 um using our method. The versatility of the approach allows for the fabrication of any type of gear systems, regardless of the configuration of individual gears or the entire system. As a result, multi-gear systems, including three, four and five gears, were also fabricated and showed stable operation.

The motor rotated under linearly polarized light, marking a notable advancement over previous methods that relied on circularly polarized or structured light to apply orbital and spin angular momentum for rotation. However, while the orientation of the metasurface determined the rotation direction, it could not be dynamically adjusted. To address this issue, I designed a new metasurface arrangement. To understand the principles for adjusting the rotation direction of the motor, it can be categorized into two distinct motors based on the distribution of the metasurface, as illustrated in Figure 5. I observed that for the top motor, the rotation direction remain clockwise under both clockwise and counterclockwise circular polarization; however, the rotation speed varied. This behavior occurred because the motor's rotation under circular polarization was contributed from two components:the torque generated by the asymmetric optical force and the spin angular momentum. When the motor rotated in the opposite direction to the circularly polarized light, the two components counteracted each other, resulting in a reduction in the motor's rotation speed. Conversely, when aligned with the light, the rotation speed of the motor increased. Based on this, when the metasurfaces of the two motors were combined into a single motor, the torque generated by the optical force was neutralized, leaving only the spin angular momentum to drive the motor's rotation. This configuration allowed the rotation direction to change in accordance with the direction of the circularly polarized light. Due to the similar structure of metasuface, the three motors were integrated onto the same substrate. By dynamically changing the polarization of light through the quarter-wave plate, the movement of the whole system changed accordingly, allowing for multiple cycles of operation.

Embedding a motor that could dynamically change its direction of rotation into a gear mechanism enabled the production of a system capable of altering its direction of movement. This capability was not limited to rotation; I also designed a gear and rack structure where the rotation of the gear drove the left and right linear movement of the rack, as shwon in Fig. 4.3f. This demonstrated that the system could effectively convert motion through a sophisticated mechanical design. However, the direction of this linear

motion needed to be determined by changing the polarization of the light, requiring the introduction of feedback control. This increased the complexity and made the system unstable. To address this issue, I modified the design by embedding a metasurface on the rack, allowing it to move in right direction under linearly polarized light, as illustrated in Fig. 4.3g. The same gear with only one tooth was coupled to the rack. When the gear contacted to the rack, the force applied by the gear exceeded the force generated by the meatsuface on the rack, pushing the rack to the left. Once separated from the rack, the rack move to the right. Through this deign, the rack can achieve reciprocating left-right linear motion under linearly polarized light. Since the system was compatible with complementary metal-oxide semiconductor (CMOS) technology, various material or structures, such as metal mirrors, could be intergrated. In this case, I introduced a micro-size gold mirror into the rack. With the linear movement of the rack, the mirror enabled dynamic scanning of light.

In summary, I developed a method to integrate light-responsive metasurfaces that drive motors on a chip, achieving sizes as small as 10um. The angular velocity of motor was controlled by light intensity, and various configuration motors can be fabricated. This motor enabled the construction of complex mechanical systems under 100um in size. Utilizing silicon as the primary material, the fabrication process was compatible with standard photolithpgraphy techniques, making commercial production feasible. This approach opens the door to a wide range of functions, providing micro- and nano-mechanical systems with unprecedented capabilities.

Contributions to the work:

In **Paper III**, I have designed the experiment and fabricated the micromachines in the cleanroom at Chalmers University of Technology. I have performed the measurement, analyzed the data and prepared manuscript and figures for publication. The optical setup that used for measurement have been built with the help of Giuseppe Pesce and Antonio Ciarlo. The thermal simulation have been performed in collaboration with Mahdi Shanei from Chalmers University of Technology.

4.4 Microscopic Motors for fluid manipulation

Building on the results from **Paper III**, we have successfully fabricated various micromachines on the chip. These micromachines can be scaled up and coordinated to operate collectively in liquid environment under the illumination. This capability has led me to consider potential applications. Upon reviewing relevant studies, I discovered that similar light-driven micromachines have been used for fluidic control, particularly as pumps in microfluidic systems [195, 73, 80, 81, 230]. However, as highlighted in background section, these devices often rely on highly focused laser beams [195, 80] or are limited to special shapes [81, 230] and large size [73], which restricts their scalability. As a result, current micromachine/micromotor-based pumps are not ideal for large-scale fluidic control or for serving as a platform adaptable to diverse fluid manipulation tasks. The micromachines develped in **Paper III** have the potential to overcome these limitations, offering a more more flexible and scalable approach for advanced fluidic control systems.

In **Paper IV**, I applied the same fabrication process from **Paper III** to fabricate micromotors with a diameter of 16 µm, which can continuously rotate under 1064 nm laser irradiation. Due to the small size and low rotational speed of the micro-motors, the fluid flow around them exhibits laminar characteristics, with fluid particles moving along parallel trajectories. This low Reynolds number flow allows the micro-motors to generate significant fluid motion with minimal force, as even small rotations or movements can induce noticeable changes in the surrounding fluid field. To map this flow, we introduced 3 µm diameters SiO_2 particles into the solution. The counterclockwise rotation of the motors caused changes in the fluid field, driving the SiO_2 particles to move in a counterclockwise direction, the schematic is shown in Fig. 4.4a. Modifying the metasurface arrangement creates a clockwise-rotating motor, which induces fluid field changes that drive SiO_2 particles' clockwise movement. Varying the rotation speeds of motor modulates the fluid dynamics, directly affecting the velocity of the SiO_2 particles.

In addition to studying the fluid field changes induced by a single motor, positioning a clockwise-rotating motor next to a counterclockwise-rotating motor generates a linear flow field. The clockwise motor creates an outward flow, while the counterclockwise motor produces an inward flow. When these flow overlap, the motors can rotate at similar speeds to maintain uniform flow, resulting in the formation of a linear flow between them (a schematic shown in Fig. 4.4b). The flow velocity is highest when the two flow fields intersect and decreases with increasing distance from this region. This outcome is illustrated by the trajectory of the SiO_2 particles, with color intensity indicating flow speed. The system is not limited to two motors; because the motors can operate under planar waves, it can be scaled up. I constructed a 2×3 motors array, with three motors on the left rotating counterclockwise and three on the right rotating clockwise, thus generating a long linear flow field. Additionally, the arrangement of the motors can be designed to create curved flow trajectories. Beside the linear flow field, positioning a clockwise-rotating motor in the center surrounded by counterclockwise-rotating motors generates a circular flow field that drives the SiO_2 particles along a circular path in the central channel.

Furthermore, this raises the question of whether fluid fields can be engineered similarly to the programming of electronic circuits. To explore this potential, I fabricated a 4×4 motor array in which the rotation direction of the 16 motors can be defined, such as clockwise or counterclockwise. When all 16 motors rotate in the same direction, the flow

field in the central region becomes zero. This occurs because the overlapping flow fields of adjacent motors cancel each other out, effectively trapping the SiO_2 particles in the center and preventing their escape. Otherwise, the surrounding 12 motors rotate in the same direction while the central 4 motors rotate in the opposite direction, a circular flow field is generated, the schematic is shown in Fig. 4.4c. Additionally, a configuration can be created where the four motors in each vertical column rotate in the opposite direction to the four motors in the adjacent vertical columns, resulting in a reciprocal flow field that closely resembles an S-shaped microfluidic channel. A more complex configuration can be established by arranging adjacent motors to rotate in opposite directions, creating an 8-shaped flow field in the central region. This design drives the SiO_2 particles to exhibit more intricate motion trajectories.

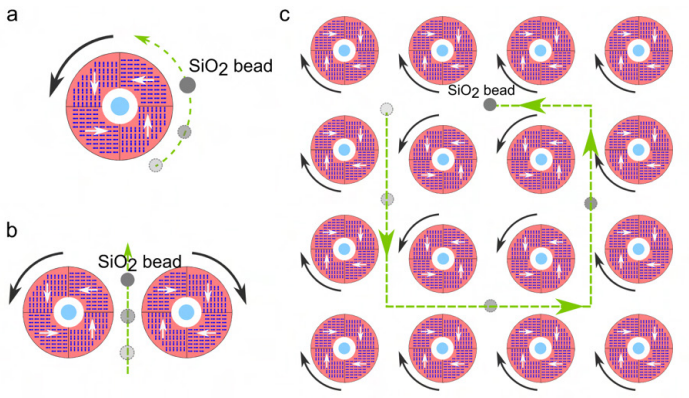

Figure 4.4: Light-driven micromotors control microparticle movement via fluid fields. a Schematic of a micromotor integrated into metasurfaces. The blue metasurface is segmented into four regions, each generating forces (white arrows) in different directions, producing optical torque. This torque drives the micromotor's counterclockwise rotation (black arrow), controlling the fluidic field to move SiO_2 particle (gray) along a counterclockwise circular trajectory (green). **b** Schematic of two micromotors rotating in opposite directions, generating a linear flow in the center. This flow drives the SiO_2 particle to move in a straight line.**c**) (Scale bars: 10 µm). **c** Schematic of a 4×4 array of micromotors with alternating rotation directions, generating a circular flow. This flow drives a particle to follow an approximately rectangular trajectory.

As previously demonstrated, the flow field changes according to the defined rotation direction of the motors. Once the rotation direction is established, the flow field is fixed. I introduced the motors demonstrated in **Paper III**, which utilize light polarization to modify their rotation direction, thereby enabling control over the flow field changes. Specially, the motors were used as gates, allowing for the control of fluid flow direction by adjusting the polarization to open or close the gates. Additionally, the motors that do not change their rotation direction were used as pumps to drive the fluid. This approach enables the reaction of a reconfigurable microfluidic chip. To conclude, motors

fabricated using microfabrication methods under planar light operation enable scaled flow field control compared to previous works. This approach allows the integration of various movement units onto the chip, facilitating the creation of functional and complex flow fields.

Contributions to the work:

In **Paper IV**, I have designed the experiment and fabricated the fluid chip in the cleanroom at Chalmers University of Technology. I have performed the measurement, analyzed the data and prepared figures and maniscript for publication. The hydrodynamic simulation have been performed in collaboration with Adrian Paskert from University of Münster.

Chapter 5

Conclusions and Future Prospects

In my research, I first used microfabrication techniques to fabricate pattern substrate, enabling the large-scale trapping and manipulation of mciron-sized particles (**Paper I**). In contrast to the method in **Paper I**, which manipulated passive particles by overcoming Brownian motion by using physical field. In **Paper II**, I further developed microfabrication techniques to construct active microswimmers that harness energy from the environment via optical fields. These microswimmers exhibited more complex behaviors. I then extended the work to micromotors integrated on the chips, designing various shapes that were coupled in gear configurations t form functional machines capable of performing complex tasks (**Paper III**). At last, these machines were applied to microfluidic control, generating complex fluid patterns under non-contact optical manipulation and were further integrated into the development of microfluidic chips (**Paper IV**).

I have shown that by designing periodic patterns composed of gold and SiO_2 on the substrate and fictionalizing thiols to alter their wettability characteristics (i.e., hydrophilic and hydrophobic), it is possible to enable these patterns to generate critical Casimir attractive and repulsive forces at the critical point in a binary liquid system due to density fluctuations as the temperature approaches the critical temperature. Both critical Casimir attractive and repulsive forces act on the particles suspended on the substrate, resulting in the trapping of these particles and allowing them to be oriented either parallel or perpendicular to the substrate. Furthermore, the transnational and rotational movements of the particles can be precisely controlled, and the shapes of the particles can be matched to the substrate patterns for effective trapping. Currently, the particles studied in **Paper I** are micro-sized, but further experiments could reduce the size to nanometers. By varying the design of pattern, such as using bull eye pattern, it is possible to trap spherical particles with diameters in the hundreds of nanometers [231]. These patterns can also be fabricated directly by etching gold using focus ion beam milling [232], offering higher precision and more complex designs compared to the lift-off fabrication process used in **Paper I**. Additionally, the patterned substrate can be used to combine with other physical field like magnetic, optical field to manipulate particles ad explore some physical phenomena, such as anomalous diffusion [233, 234], friction [235, 236]. In the experiment, I used 100× oil-immersion objective to control the temperature, with the heat being conducted from the objective through the immersion oil to the sample. The area of temperature control was limited by the contact area of the objective, restricting the scalability of the system. To address this limitation, conductive substrates such as ITO glass [237] or gold substrate [238]

could be used, allowing the sample to be heated via electric current. This would eliminate the requirement for heavy objective and enable wafer-scale particle manipulation.

In **I**, I controlled disk-shaped particles, which hold potential for various applications, including the micro-LED self assemble. Micro-LEDS are typically grown on sapphire substrates to ensure high quality but must be transferred to silicon substrates for circuit integration. Thus, large-scale transfer is crucial [239]. Currently, the commercial transfer process relies on laser pulse [240], but limited throughput hinders widespread application. **Paper I** demonstrated a temperature-controlled transfer method. If this method could be scaled up, it would enable high-throughput transfer of micro-LED disk-shaped particles. Additionally, the design of the substrate patterns affects particle's trapping, allowing for the trapping of particles of different sizes and shapes, facilitating the simultaneous assembly of RGB particles with distinct advantages. Moreover, beyond the two-dimensional alignment of particles, this approach can be extended to three-dimensional assemblies, analogous to work using the Casimir and electrostatic force enables the stacking of multiple particles along the Z-axis [241]. In this system, the diversity in particle shapes and compositions can be achieved through microfabrication techniques, offering greater potential for the development of functional devices via three-dimensional assembly.

I have shown that metasurfaces can be embedded into microparticles through microfabrication techniques such as photolithography and etching. These metasurfaces can manipulate optical fields to facilitate momentum exchange between light and particles, enabling particle movement in water. By controlling the distribution of metasurfaces on the particles, the light intensity, and the shape of the microswimmers, a wide range of behavioral patterns can be achieved. Furthermore, these behaviors can be regulated by adjusting the polarization of the light. The long-term goal of microswimmers is to develop capabilities similar to bacteria, such as environmental sensing, information transmission, and diverse motion abilities [242]. Although progress has been made in diversifying their motion [243], the development of other capabilities remains limited. In **Paper II**, the production of particles compatible with standard semiconductor processes can be further functionalized by depositing materials that are sensitive to temperature, light, or chemicals to achieve these additional functionalities. For example, by depositing temperature-sensitive VO_2 on the metasurface, the refractive index and optical transmission can be modified by temperature changes [244], affecting the metasurface's diffraction efficiency and subsequently the microswimmer's behavior. This enables microswimmers to adapt their behavior based on environmental changes. Moreover, environment-sensitive polymers can be functionalized on the surface of the microswimmers, where changes in pH [245] or temperature [246] cause transitions in polymer configuration, such as from an upright to a collapsed state, altering the drag on the microswimmers in liquid and consequently influencing their movement. Additionally, microswimmers can be connected by these polymers, such as hydrogels [68] or liquid crystals [247], which can be achieved using two-photon lithography techniques. By controlling the configuration of these polymers between microswimmers, the overall shape and behavior of the microswimmers can be modulated. This approach could even be extended to design origami-like structures [248], creating mechanical metamaterials [249, 250]. Given the powerful capabilities of microfabrication technologies, many functional microstructures can be integrated into microswimmers to enable more intelligent behaviors.

In **Paper III**, I have shown a micromotor that uses metasurface, as in **Paper II**,

to enable momentum exchange between light and motor, allowing for rotation. The key advancement was the integration of the micromotor onto a chip using newly developed microfabrication techniques. By shaping the micromotor as a gear, it became possible to couple it with other gears, forming more complex machines. In this system, gears with metasurfaces act as driven gears, while those without function as passive gears. When illuminated, the driven gear rotates and drives the passive ones. The number of gears can be scaled from one to five or more. Furthermore, the micromotor was designed to rotate either clockwise or counterclockwise, depending on the polarization of light. Beyond simple rotation, the gear system can be combined with a rack to convert rotational motion into linear movement. The fabrication process is fully compatible with CMOS methods, which allows gold mirrors to be embedded into the structure to facilitate optical beam scanning. As discussed in the background section, this work addresses the size limitations of earlier electrostatic-driven machines. In comparison to existing far-field driven methods, which are mainly limited to single motors due to challenges in compatibility with commercial microfabrication, this approach demonstrates the feasibility of coupling multiple motors to form functional machines. In the **Paper III**, the movement of micromotor is not constrained by its shape, as the movement is primarily determined by the metasurface embedded within the motor. This allows for the production of machines with any configuration at this scale. In general, this system provides a versatile platform that can adapted to meet the need of other fields such as mechanical engineering, chemistry, and biology. The micromotor can be tailored to construct machine configurations required for specific research applications. Given its cell-szied dimensions, the motor could function as a highly sensitive sensor capable of measuring biomechanical forces [251]. Furthermore, due to its compatibility with CMOS technology, the micromotor could be integrated with optical, electrical, and chemical sensors, enabling precise detection of environmental analytes or compounds.

The work has shown in **Paper III** is the application of micromachine developed in **Paper II**. The rotation of the motor induces fluid movement, facilitating transport of particles. Through microfabrication techniques, motors with adjustable configurations and distance can be positioned on the same chip and operated simultaneously under illumination. Various motor arrays have been designed, making complex fluid manipulation feasible. Current efforts focus on controlling fluid dynamics, using a small number of colloidal particles as tracers to visualize the fluid flow. Future work could involve denser particle systems to study their collective behavior [150] under fluidic control. Additionally, luminescent particles could be introduced, allowing the system to act as a microdevice for modulating light fields. This setup could also function as an optical tweezers to control the alignment of particles like cellulose [252], potentially coupling with other devices to explore their properties.

Acknowledgement

First and foremost, I want to thank my main supervisor, Prof. Giovanni Volpe, for giving me the opportunity to begin my PhD journey at Gothenburg University. As the supervisor of my project, he provided me with invaluable support and encouragement, allowing me to freely explore topics that interested me. Your brilliance and guidance have been crucial throughout my studies. I also wish to express my heartfelt thanks to my co-supervisor, Prof. Mikael Käll. Your relentless passion and dedication to research have been a constant source of inspiration to me.

I would like to sincerely thank all the people involved in the projects I've conducted during my PhD studies. Mahdi, it has been a pleasure working with you in the cleanroom and on our shared projects over the past four years. These experiences will always be cherished memories for me. I wish you all the best and hope you enjoy your new job. Marcel and Kunli, our discussions have provided me with new perspectives and inspiration for my research. I wish you both the best of luck in your academic journeys. Antonio and Peppe, thank you so much for your help with the optical setup. I have learned a great deal about optics from both of you. Ruggero, I appreciate your teaching and support in nanofabrication. Piotr, Slava, Adrian, Raphael, Edoardo, Agnese, and Benjamin, thank you for your support and guidance with the theoretical aspects of our projects. To all the other collaborators, thank you for your valuable discussions and assistance, from which I have learned immensely.

Also, I want to thank all the past and present group members of the soft matter lab. Thank you for your support and advice, you are always wiling to share ideas with me, even chatting with me over fika, these moments make me feel special and warm in this journey. Hari, Yuwei, Hang, Martin, Harshith, Charlotte, Caroline, Laura and all others. Thank you. And Hari, I am excited to see your powerful soft robots in action.

I would like to thank the friends I met outside the lab in Sweden, Xinwei, Zhejian, Mufei, Peng, Hanlin, and others. The travels and discussions we had together made this journey much more enjoyable and fulfilling.

Moreover, I am thankful to all the people working in cleanroom for your valuable support and guidance.

Finally, I would like to express my deepest gratitude to my loving wife and family. Your unwavering support and encouragement have been the driving force behind this journey, making it not only possible but also truly meaningful and unforgettable. Thank you for being my source of strength and inspiration every step of the way.

References

[1] A. Einstein, *Zur Quantentheorie der Strahlung*, Verlag u. Druck Gebr. Leemann, Berlin (1916).

[2] T. H. Maiman*et al.*, Stimulated optical radiation in ruby, *Nature* **187**, 493–494 (1960).

[3] T. Udem, R. Holzwarth, and T. W. Hänsch, Optical frequency metrology, *Nature* **416**, 233–237 (2002).

[4] H. J. Metcalf and P. Van der Straten, *Laser cooling and trapping*, Springer Science & Business Media (1999).

[5] A. Ashkin, Acceleration and trapping of particles by radiation pressure, *Physical Review Letters* **24**, 156 (1970).

[6] M. M. Waldrop, The chips are down for Moore's law, *Nature News* **530**, 144 (2016).

[7] W. Cao, H. Bu, M. Vinet, M. Cao, S. Takagi, S. Hwang, T. Ghani, and K. Banerjee, The future transistors, *Nature* **620**, 501–515 (2023).

[8] H. J. Levinson, *Principles of lithography*, volume 146, SPIE press (2005).

[9] M.-H. Bao, *Micro mechanical transducers: pressure sensors, accelerometers and gyroscopes*, Elsevier (2000).

[10] D. Wang, C. Watkins, and H. Xie, MEMS mirrors for LiDAR: A review, *Micromachines* **11**, 456 (2020).

[11] F. Arai, D. Andou, Y. Nonoda, T. Fukuda, H. Iwata, and K. Itoigawa, Integrated microendeffector for micromanipulation, *IEEE/ASME transactions on mechatronics* **3**, 17–23 (1998).

[12] Y. Xia and G. M. Whitesides, Soft lithography, *Angewandte Chemie International Edition* **37**, 550–575 (1998).

[13] F. W. DelRio, M. P. De Boer, J. A. Knapp, E. David Reedy Jr, P. J. Clews, and M. L. Dunn, The role of van der Waals forces in adhesion of micromachined surfaces, *Nature Materials* **4**, 629–634 (2005).

[14] H. B. Chan, V. A. Aksyuk, R. N. Kleiman, D. J. Bishop, and F. Capasso, Quantum mechanical actuation of microelectromechanical systems by the Casimir force, *Science* **291**, 1941–1944 (2001).

[15] S. H. Kim, D. B. Asay, and M. T. Dugger, Nanotribology and MEMS, *Nano Today* **2**, 22–29 (2007).

[16] S. Jin, J. Li, J. Li, J. Lin, and H. Jiang, GaN microdisk light emitting diodes, *Applied Physics Letters* **76**, 631–633 (2000).

[17] M. Khorasaninejad, W. T. Chen, R. C. Devlin, J. Oh, A. Y. Zhu, and F. Capasso, Metalenses at visible wavelengths: Diffraction-limited focusing and subwavelength resolution imaging, *Science* **352**, 1190–1194 (2016).

[18] L. Gu, S. Poddar, Y. Lin, Z. Long, D. Zhang, Q. Zhang, L. Shu, X. Qiu, M. Kam, A. Javey,*et al.*, A biomimetic eye with a hemispherical perovskite nanowire array retina, *Nature* **581**, 278–282 (2020).

[19] J. Foresi, P. R. Villeneuve, J. Ferrera, E. Thoen, G. Steinmeyer, S. Fan, J. Joannopoulos, L. Kimerling, H. I. Smith, and E. Ippen, Photonic-bandgap microcavities in optical waveguides, *Nature* **390**, 143–145 (1997).

[20] R. Feynman, There's plenty of room at the bottom, In *Feynman and Computation*, pages 63–76, CRC Press (2018).

[21] M. Nirmal and L. Brus, Luminescence photophysics in semiconductor nanocrystals, *Accounts of Chemical Research* **32**, 407–414 (1999).

[22] M. L. Juan, M. Righini, and R. Quidant, Plasmon nano-optical tweezers, *Nature Photonics* **5**, 349–356 (2011).

[23] O. M. Marago, P. H. Jones, P. G. Gucciardi, G. Volpe, and A. C. Ferrari, Optical trapping and manipulation of nanostructures, *Nature Nanotechnology* **8**, 807–819 (2013).

[24] M. Z. Miskin, A. J. Cortese, K. Dorsey, E. P. Esposito, M. F. Reynolds, Q. Liu, M. Cao, D. A. Muller, P. L. McEuen, and I. Cohen, Electronically integrated, mass-manufactured, microscopic robots, *Nature* **584**, 557–561 (2020).

[25] J. Cui, T.-Y. Huang, Z. Luo, P. Testa, H. Gu, X.-Z. Chen, B. J. Nelson, and L. J. Heyderman, Nanomagnetic encoding of shape-morphing micromachines, *Nature* **575**, 164–168 (2019).

[26] W. Wang, Q. Liu, I. Tanasijevic, M. F. Reynolds, A. J. Cortese, M. Z. Miskin, M. C. Cao, D. A. Muller, A. C. Molnar, E. Lauga,*et al.*, Cilia metasurfaces for electronically programmable microfluidic manipulation, *Nature* **605**, 681–686 (2022).

[27] P. J. Pauzauskie, A. Radenovic, E. Trepagnier, H. Shroff, P. Yang, and J. Liphardt, Optical trapping and integration of semiconductor nanowire assemblies in water, *Nature Materials* **5**, 97–101 (2006).

[28] Y. Nakayama, P. J. Pauzauskie, A. Radenovic, R. M. Onorato, R. J. Saykally, J. Liphardt, and P. Yang, Tunable nanowire nonlinear optical probe, *Nature* **447**, 1098–1101 (2007).

[29] A. F. Demirörs, P. P. Pillai, B. Kowalczyk, and B. A. Grzybowski, Colloidal assembly directed by virtual magnetic moulds, *Nature* **503**, 99–103 (2013).

[30] B. Li, D. Zhou, and Y. Han, Assembly and phase transitions of colloidal crystals, *Nature Reviews Materials* **1**, 1–13 (2016).

[31] C. Liu, K. Kubo, E. Wang, K.-S. Han, F. Yang, G. Chen, F. A. Escobedo, G. W. Coates, and P. Chen, Single polymer growth dynamics, *Science* **358**, 352–355 (2017).

[32] Q. Cao, Q. Fan, Q. Chen, C. Liu, X. Han, and L. Li, Recent advances in manipulation of micro-and nano-objects with magnetic fields at small scales, *Materials Horizons* **7**, 638–666 (2020).

[33] R. S. Rikken, R. J. Nolte, J. C. Maan, J. C. van Hest, D. A. Wilson, and P. C. Christianen, Manipulation of micro-and nanostructure motion with magnetic fields, *Soft Matter* **10**, 1295–1308 (2014).

[34] A. Snezhko and I. S. Aranson, Magnetic manipulation of self-assembled colloidal asters, *Nature Materials* **10**, 698–703 (2011).

[35] M. Sun, S. Yang, J. Jiang, S. Jiang, M. Sitti, and L. Zhang, Bioinspired self-assembled colloidal collectives drifting in three dimensions underwater, *Science Advances* **9**, eadj4201 (2023).

[36] A. Ashkin, J. M. Dziedzic, J. E. Bjorkholm, and S. Chu, Observation of a single-beam gradient force optical trap for dielectric particles, *Optics Letters* **11**, 288–290 (1986).

[37] S. Paladugu, A. Callegari, Y. Tuna, L. Barth, S. Dietrich, A. Gambassi, and G. Volpe, Nonadditivity of critical Casimir forces, *Nature communications* **7**, 11403 (2016).

[38] J. Berthelot, S. S. Aćimović, M. L. Juan, M. P. Kreuzer, J. Renger, and R. Quidant, Three-dimensional manipulation with scanning near-field optical nanotweezers, *Nature Nanotechnology* **9**, 295–299 (2014).

[39] P. Jones, O. Maragó, and G. Volpe, *Optical tweezers*, Cambridge University Press Cambridge (2015).

[40] M. Krishnan, N. Mojarad, P. Kukura, and V. Sandoghdar, Geometry-induced electrostatic trapping of nanometric objects in a fluid, *Nature* **467**, 692–695 (2010).

[41] A. P. Fields and A. E. Cohen, Electrokinetic trapping at the one nanometer limit, *Proceedings of the National Academy of Sciences* **108**, 8937–8942 (2011).

[42] H. Li, D. Teal, Z. Liang, H. Kwon, D. Huo, A. Jin, P. Fischer, and D. E. Fan, Precise electrokinetic position and three-dimensional orientation control of a nanowire bioprobe in solution, *Nature Nanotechnology* **18**, 1213–1221 (2023).

[43] O. D. Velev and K. H. Bhatt, On-chip micromanipulation and assembly of colloidal particles by electric fields, *Soft Matter* **2**, 738–750 (2006).

[44] Y. Jin, W. Xu, H. Zhang, R. Li, J. Sun, S. Yang, M. Liu, H. Mao, and Z. Wang, Electrostatic tweezer for droplet manipulation, *Proceedings of the National Academy of Sciences* **119**, e2105459119 (2022).

[45] A. Maciołek and S. Dietrich, Collective behavior of colloids due to critical Casimir interactions, *Reviews of Modern Physics* **90**, 045001 (2018).

[46] C. Hertlein, L. Helden, A. Gambassi, S. Dietrich, and C. Bechinger, Direct measurement of critical Casimir forces, *Nature* **451**, 172–175 (2008).

[47] M. Fukuto, Y. F. Yano, and P. S. Pershan, Critical Casimir Effect in Three-Dimensional Ising Systems:¡? format?¿ Measurements on Binary Wetting Films, *Physical Review Letters* **94**, 135702 (2005).

[48] V. D. Nguyen, S. Faber, Z. Hu, G. H. Wegdam, and P. Schall, Controlling colloidal phase transitions with critical Casimir forces, *Nature Communications* **4**, 1584 (2013).

[49] P. J. Swinkels, Z. Gong, S. Sacanna, E. G. Noya, and P. Schall, Visualizing defect dynamics by assembling the colloidal graphene lattice, *Nature Communications* **14**, 1524 (2023).

[50] F. Schmidt, A. Callegari, A. Daddi-Moussa-Ider, B. Munkhbat, R. Verre, T. Shegai, M. Käll, H. Löwen, A. Gambassi, and G. Volpe, Tunable critical Casimir forces counteract Casimir–Lifshitz attraction, *Nature Physics* **19**, 271–278 (2023).

[51] A. Gambassi and S. Dietrich, Critical Casimir forces steered by patterned substrates, *Soft Matter* **7**, 1247–1253 (2011).

[52] F. Soyka, O. Zvyagolskaya, C. Hertlein, L. Helden, and C. Bechinger, Critical Casimir forces in colloidal suspensions on chemically patterned surfaces, *Physical Review Letters* **101**, 208301 (2008).

[53] W. F. Paxton, P. T. Baker, T. R. Kline, Y. Wang, T. E. Mallouk, and A. Sen, Catalytically induced electrokinetics for motors and micropumps, *Journal of the American Chemical Society* **128**, 14881–14888 (2006).

[54] S. Sánchez, L. Soler, and J. Katuri, Chemically powered micro-and nanomotors, *Angewandte Chemie International Edition* **54**, 1414–1444 (2015).

[55] W. Gao, A. Pei, R. Dong, and J. Wang, Catalytic iridium-based Janus micromotors powered by ultralow levels of chemical fuels, *Journal of the American Chemical Society* **136**, 2276–2279 (2014).

[56] W. Gao, A. Pei, and J. Wang, Water-driven micromotors, *ACS Nano* **6**, 8432–8438 (2012).

[57] S. Gangwal, O. J. Cayre, M. Z. Bazant, and O. D. Velev, Induced-charge electrophoresis of metallodielectric particles, *Physical Review Letters* **100**, 058302 (2008).

[58] J. Yan, M. Han, J. Zhang, C. Xu, E. Luijten, and S. Granick, Reconfiguring active particles by electrostatic imbalance, *Nature Materials* **15**, 1095–1099 (2016).

[59] J. Zhang, R. Alert, J. Yan, N. S. Wingreen, and S. Granick, Active phase separation by turning towards regions of higher density, *Nature Physics* **17**, 961–967 (2021).

[60] S. Tottori, L. Zhang, F. Qiu, K. K. Krawczyk, A. Franco-Obregón, and B. J. Nelson, Magnetic helical micromachines: fabrication, controlled swimming, and cargo transport, *Advanced Materials* **24**, 811–816 (2012).

[61] Z. Wu, J. Troll, H.-H. Jeong, Q. Wei, M. Stang, F. Ziemssen, Z. Wang, M. Dong, S. Schnichels, T. Qiu,*et al.*, A swarm of slippery micropropellers penetrates the vitreous body of the eye, *Science Advances* **4**, eaat4388 (2018).

[62] J. Yan, M. Bloom, S. C. Bae, E. Luijten, and S. Granick, Linking synchronization to self-assembly using magnetic Janus colloids, *Nature* **491**, 578–581 (2012).

[63] Y. Alapan, B. Yigit, O. Beker, A. F. Demirörs, and M. Sitti, Shape-encoded dynamic assembly of mobile micromachines, *Nature Materials* **18**, 1244–1251 (2019).

[64] A. Aghakhani, O. Yasa, P. Wrede, and M. Sitti, Acoustically powered surface-slipping mobile microrobots, *Proceedings of the National Academy of Sciences* **117**, 3469–3477 (2020).

[65] M. Valdez-Garduño, M. Leal-Estrada, E. S. Oliveros-Mata, D. I. Sandoval-Bojorquez, F. Soto, J. Wang, and V. Garcia-Gradilla, Density asymmetry driven propulsion of ultrasound-powered Janus micromotors, *Advanced Functional Materials* **30**, 2004043 (2020).

[66] Y. Deng, A. Paskert, Z. Zhang, R. Wittkowski, and D. Ahmed, An acoustically controlled helical microrobot, *Science Advances* **9**, eadh5260 (2023).

[67] F. Kümmel, B. Ten Hagen, R. Wittkowski, I. Buttinoni, R. Eichhorn, G. Volpe, H. Löwen, and C. Bechinger, Circular motion of asymmetric self-propelling particles, *Physical Review Letters* **110**, 198302 (2013).

[68] H. Zhang, L. Koens, E. Lauga, A. Mourran, and M. Möller, A Light-Driven Microgel Rotor, *Small* **15**, 1903379 (2019).

[69] X. Peng, Z. Chen, P. S. Kollipara, Y. Liu, J. Fang, L. Lin, and Y. Zheng, Opto-thermoelectric microswimmers, *Light: Science & Applications* **9**, 141 (2020).

[70] D. Bronte Ciriza, A. Callegari, M. G. Donato, B. Çiçek, A. Magazzù, I. Kasianiuk, D. Kasyanyuk, F. Schmidt, A. Foti, P. G. Gucciardi,*et al.*, Optically driven Janus microengine with full orbital motion control, *ACS Photonics* **10**, 3223–3232 (2023).

[71] D. Andrén, D. G. Baranov, S. Jones, G. Volpe, R. Verre, and M. Käll, Microscopic metavehicles powered and steered by embedded optical metasurfaces, *Nature Nanotechnology* **16**, 970–974 (2021).

[72] P. Galajda and P. Ormos, Complex micromachines produced and driven by light, *Applied Physics Letters* **78**, 249–251 (2001).

[73] S. Zhang, M. Elsayed, R. Peng, Y. Chen, Y. Zhang, J. Peng, W. Li, M. D. Chamberlain, A. Nikitina, S. Yu,*et al.*, Reconfigurable multi-component micromachines driven by optoelectronic tweezers, *Nature Communications* **12**, 5349 (2021).

[74] S. Haeberle and R. Zengerle, Microfluidic platforms for lab-on-a-chip applications, *Lab on a Chip* **7**, 1094–1110 (2007).

[75] D. J. Beebe, G. A. Mensing, and G. M. Walker, Physics and applications of microfluidics in biology, *Annual Review of Biomedical Engineering* **4**, 261–286 (2002).

[76] K. S. Elvira, X. C. i Solvas, R. C. Wootton, and A. J. Demello, The past, present and potential for microfluidic reactor technology in chemical synthesis, *Nature Chemistry* **5**, 905–915 (2013).

[77] N.-T. Nguyen, X. Huang, and T. K. Chuan, MEMS-micropumps: a review, *J. Fluids Eng.* **124**, 384–392 (2002).

[78] D. J. Laser and J. G. Santiago, A review of micropumps, *Journal of Micromechanics and Microengineering* **14**, R35 (2004).

[79] P. Woias, Micropumps—past, progress and future prospects, *Sensors and Actuators B: Chemical* **105**, 28–38 (2005).

[80] S. Maruo and H. Inoue, Optically driven viscous micropump using a rotating microdisk, *Applied Physics Letters* **91** (2007).

[81] U. G. Būtaitė, G. M. Gibson, Y.-L. D. Ho, M. Taverne, J. M. Taylor, and D. B. Phillips, Indirect optical trapping using light driven micro-rotors for reconfigurable hydrodynamic manipulation, *Nature Communications* **10**, 1215 (2019).

[82] R. Brown, 29 A brief account of microscopical observations made in the months of June, July and August 1827 on the particles contained in the pollen of plants; and on the general existence of active molecules in organic and inorganic bodies, *Not published at the time but printed in Miscellaneous botanical works of Robert Brown, ed. JJ Bennett, Ray Society* **1866**, 465 (1828).

[83] E. Nelson, *Dynamical theories of Brownian motion*, volume 101, Princeton university press (2020).

[84] P. Mörters and Y. Peres, *Brownian motion*, volume 30, Cambridge University Press (2010).

[85] J. Ahn, Z. Xu, J. Bang, Y.-H. Deng, T. M. Hoang, Q. Han, R.-M. Ma, and T. Li, Optically levitated nanodumbbell torsion balance and GHz nanomechanical rotor, *Physical review letters* **121**, 033603 (2018).

[86] F. Grillo, M. A. Fernandez-Rodriguez, M.-N. Antonopoulou, D. Gerber, and L. Isa, Self-templating assembly of soft microparticles into complex tessellations, *Nature* **582**, 219–224 (2020).

[87] J. Li and Y. Zheng, Optothermally assembled nanostructures, *Accounts of materials research* **2**, 352–363 (2021).

[88] S. Yang, Z. Tian, Z. Wang, J. Rufo, P. Li, J. Mai, J. Xia, H. Bachman, P.-H. Huang, M. Wu,*et al.*, Harmonic acoustics for dynamic and selective particle manipulation, *Nature materials* **21**, 540–546 (2022).

[89] B. Melo, M. T. Cuairan, G. F. Tomassi, N. Meyer, and R. Quidant, Vacuum levitation and motion control on chip, *Nature Nanotechnology* pages 1–7 (2024).

[90] F. Tebbenjohanns, M. L. Mattana, M. Rossi, M. Frimmer, and L. Novotny, Quantum control of a nanoparticle optically levitated in cryogenic free space, *Nature* **595**, 378–382 (2021).

[91] J. C. Crocker and D. G. Grier, Microscopic measurement of the pair interaction potential of charge-stabilized colloid, *Physical review letters* **73**, 352 (1994).

[92] J. C. Crocker, J. A. Matteo, A. D. Dinsmore, and A. G. Yodh, Entropic attraction and repulsion in binary colloids probed with a line optical tweezer, *Physical review letters* **82**, 4352 (1999).

[93] G. Vieira, T. Henighan, A. Chen, A. Hauser, F. Yang, J. Chalmers, and R. Sooryakumar, Magnetic wire traps and programmable manipulation of biological cells, *Physical review letters* **103**, 128101 (2009).

[94] P. Y. Chiou, A. T. Ohta, and M. C. Wu, Massively parallel manipulation of single cells and microparticles using optical images, *Nature* **436**, 370–372 (2005).

[95] C. J. Bustamante, Y. R. Chemla, S. Liu, and M. D. Wang, Optical tweezers in single-molecule biophysics, *Nature Reviews Methods Primers* **1**, 25 (2021).

[96] J. Lipfert, J. W. Kerssemakers, T. Jager, and N. H. Dekker, Magnetic torque tweezers: measuring torsional stiffness in DNA and RecA-DNA filaments, *Nature methods* **7**, 977–980 (2010).

[97] S. Zhang, Y. Wang, P. Onck, and J. den Toonder, A concise review of microfluidic particle manipulation methods, *Microfluidics and Nanofluidics* **24**, 24 (2020).

[98] A. Miyagawa and T. Okada, Particle manipulation with external field; from recent advancement to perspectives, *Analytical Sciences* **37**, 69–78 (2021).

[99] K. Cheng, J. Guo, Y. Fu, and J. Guo, Active microparticle manipulation: Recent advances, *Sensors and Actuators A: Physical* **322**, 112616 (2021).

[100] K. Melde, H. Kremer, M. Shi, S. Seneca, C. Frey, I. Platzman, C. Degel, D. Schmitt, B. Schölkopf, and P. Fischer, Compact holographic sound fields enable rapid one-step assembly of matter in 3D, *Science Advances* **9**, eadf6182 (2023).

[101] P. Zhang, H. Bachman, A. Ozcelik, and T. J. Huang, Acoustic microfluidics, *Annual Review of Analytical Chemistry* **13**, 17–43 (2020).

[102] M. Baudoin and J.-L. Thomas, Acoustic tweezers for particle and fluid micromanipulation, *Annual Review of Fluid Mechanics* **52**, 205–234 (2020).

[103] A. G. Athanassiadis, Z. Ma, N. Moreno-Gomez, K. Melde, E. Choi, R. Goyal, and P. Fischer, Ultrasound-responsive systems as components for smart materials, *Chemical reviews* **122**, 5165–5208 (2021).

[104] J. Li, Z. Chen, Y. Liu, P. S. Kollipara, Y. Feng, Z. Zhang, and Y. Zheng, Opto-refrigerative tweezers, *Science Advances* **7**, eabh1101 (2021).

[105] L. Lin, M. Wang, X. Peng, E. N. Lissek, Z. Mao, L. Scarabelli, E. Adkins, S. Coskun, H. E. Unalan, B. A. Korgel,*et al.*, Opto-thermoelectric nanotweezers, *Nature Photonics* **12**, 195–201 (2018).

[106] M. Fränzl and F. Cichos, Hydrodynamic manipulation of nano-objects by optically induced thermo-osmotic flows, *Nature Communications* **13**, 656 (2022).

[107] M. Braun and F. Cichos, Optically controlled thermophoretic trapping of single nano-objects, *ACS Nano* **7**, 11200–11208 (2013).

[108] H.-R. Jiang, H. Wada, N. Yoshinaga, and M. Sano, Manipulation of colloids by a nonequilibrium depletion force in a temperature gradient, *Physical Review Letters* **102**, 208301 (2009).

[109] R. Merritt, C. Purcell, and G. Stroink, Uniform magnetic field produced by three, four, and five square coils, *Review of Scientific Instruments* **54**, 879–882 (1983).

[110] E. Danieli, J. Perlo, B. Blümich, and F. Casanova, Highly stable and finely tuned magnetic fields generated by permanent magnet assemblies, *Physical review letters* **110**, 180801 (2013).

[111] Q. Cao, X. Han, and L. Li, Configurations and control of magnetic fields for manipulating magnetic particles in microfluidic applications: magnet systems and manipulation mechanisms, *Lab on a Chip* **14**, 2762–2777 (2014).

[112] K.-B. Lee, S. Park, C. A. Mirkin,*et al.*, Multicomponent magnetic nanorods for biomolecular separations, *Angewandte Chemie International Edition* **43**, 3048–3050 (2004).

[113] R. Eivazzadeh-Keihan, H. Bahreinizad, Z. Amiri, H. A. M. Aliabadi, M. Salimi-Bani, A. Nakisa, F. Davoodi, B. Tahmasebi, F. Ahmadpour, F. Radinekiyan,*et al.*, Functionalized magnetic nanoparticles for the separation and purification of proteins and peptides, *TrAC Trends in Analytical Chemistry* **141**, 116291 (2021).

[114] H.-K. Choi, H. G. Kim, M. J. Shon, and T.-Y. Yoon, High-resolution single-molecule magnetic tweezers, *Annual Review of Biochemistry* **91**, 33–59 (2022).

[115] N. Ribeck and O. A. Saleh, Multiplexed single-molecule measurements with magnetic tweezers, *Review of Scientific Instruments* **79** (2008).

[116] B. Sarno, D. Heineck, M. J. Heller, and S. D. Ibsen, Dielectrophoresis: Developments and applications from 2010 to 2020, *Electrophoresis* **42**, 539–564 (2021).

[117] W. Waheed, A. Alazzam, A. N. Al-Khateeb, and E. Abu-Nada, Multiple particle manipulation under dielectrophoresis effect: Modeling and experiments, *Langmuir* **36**, 3016–3028 (2020).

[118] K. Yu, Electrophoresis-based manipulation of micro-and nanoparticles in fluid suspensions, *Field-Driven Micro and Nanorobots for Biology and Medicine* pages 133–164 (2022).

[119] J. Wu, Biased AC electro-osmosis for on-chip bioparticle processing, *IEEE Transactions on Nanotechnology* **5**, 84–89 (2006).

[120] K. Kim, X. Xu, J. Guo, and D. Fan, Ultrahigh-speed rotating nanoelectromechanical system devices assembled from nanoscale building blocks, *Nature communications* **5**, 3632 (2014).

[121] T. B. Jones, Electromechanics of particles, *(No Title)* (1995).

[122] Z. Wang and J. Zhe, Recent advances in particle and droplet manipulation for lab-on-a-chip devices based on surface acoustic waves, *Lab on a Chip* **11**, 1280–1285 (2011).

[123] H. Bruus, Acoustofluidics 7: The acoustic radiation force on small particles, *Lab on a Chip* **12**, 1014–1021 (2012).

[124] K. Dholakia, B. W. Drinkwater, and M. Ritsch-Marte, Comparing acoustic and optical forces for biomedical research, *Nature Reviews Physics* **2**, 480–491 (2020).

[125] G. T. Silva and H. Bruus, Acoustic interaction forces between small particles in an ideal fluid, *Physical Review E* **90**, 063007 (2014).

[126] X. Ding, S.-C. S. Lin, B. Kiraly, H. Yue, S. Li, I.-K. Chiang, J. Shi, S. J. Benkovic, and T. J. Huang, On-chip manipulation of single microparticles, cells, and organisms using surface acoustic waves, *Proceedings of the National Academy of Sciences* **109**, 11105–11109 (2012).

[127] M. A. Andrade, A. Marzo, and J. C. Adamowski, Acoustic levitation in mid-air: Recent advances, challenges, and future perspectives, *Applied Physics Letters* **116** (2020).

[128] C. Yin, X. Jiang, S. Mann, L. Tian, and B. W. Drinkwater, Acoustic trapping: An emerging tool for microfabrication technology, *Small* **19**, 2207917 (2023).

[129] D. J. Wineland and W. M. Itano, Laser cooling of atoms, *Physical Review A* **20**, 1521 (1979).

[130] C. Zhan, G. Wang, J. Yi, J.-Y. Wei, Z.-H. Li, Z.-B. Chen, J. Shi, Y. Yang, W. Hong, and Z.-Q. Tian, Single-molecule plasmonic optical trapping, *Matter* **3**, 1350–1360 (2020).

[131] D. G. Grier, Optical tweezers in colloid and interface science, *Current opinion in colloid & interface science* **2**, 264–270 (1997).

[132] M. C. Wu, Optoelectronic tweezers, *Nature Photonics* **5**, 322–324 (2011).

[133] S. Zhang, B. Xu, M. Elsayed, F. Nan, W. Liang, J. K. Valley, L. Liu, Q. Huang, M. C. Wu, and A. R. Wheeler, Optoelectronic tweezers: a versatile toolbox for nano-/micro-manipulation, *Chemical Society Reviews* **51**, 9203–9242 (2022).

[134] Z. Chen, J. Li, and Y. Zheng, Heat-mediated optical manipulation, *Chemical Reviews* **122**, 3122–3179 (2021).

[135] G. Baffou, F. Cichos, and R. Quidant, Applications and challenges of thermoplasmonics, *Nature Materials* **19**, 946–958 (2020).

[136] M. Fränzl, T. Thalheim, J. Adler, D. Huster, J. Posseckardt, M. Mertig, and F. Cichos, Thermophoretic trap for single amyloid fibril and protein aggregation studies, *Nature Methods* **16**, 611–614 (2019).

[137] A. A. Hyman, C. A. Weber, and F. Jülicher, Liquid-liquid phase separation in biology, *Annual review of cell and developmental biology* **30**, 39–58 (2014).

[138] C. A. Grattoni, R. A. Dawe, C. Y. Seah, and J. D. Gray, Lower critical solution coexistence curve and physical properties (density, viscosity, surface tension, and interfacial tension) of 2, 6-lutidine+ water, *Journal of Chemical and Engineering Data* **38**, 516–519 (1993).

[139] M. E. Fisher and P.-G. de Gennes, Wall phenomena in a critical binary mixture, *CR Acad. Sci. Paris B* **287**, 207–209 (1978).

[140] H. B. Casimir and D. Polder, The influence of retardation on the London-van der Waals forces, *Physical Review* **73**, 360 (1948).

[141] W. M. Van Spengen, R. Puers, and I. De Wolf, The prediction of stiction failures in MEMS, *IEEE Transactions on Device and Materials reliability* **3**, 167–172 (2003).

[142] A. W. Rodriguez, F. Capasso, and S. G. Johnson, The Casimir effect in microstructured geometries, *Nature photonics* **5**, 211–221 (2011).

[143] E. M. Lifshitz, M. Hamermesh,*et al.*, The theory of molecular attractive forces between solids, In *Perspectives in Theoretical Physics*, pages 329–349, Elsevier (1992).

[144] J. N. Munday, F. Capasso, and V. A. Parsegian, Measured long-range repulsive Casimir–Lifshitz forces, *Nature* **457**, 170–173 (2009).

[145] A. Gambassi, A. Maciołek, C. Hertlein, U. Nellen, L. Helden, C. Bechinger, and S. Dietrich, Critical Casimir effect in classical binary liquid mixtures, *Physical Review E—Statistical, Nonlinear, and Soft Matter Physics* **80**, 061143 (2009).

[146] U. Mohideen and A. Roy, Precision measurement of the Casimir force from 0.1 to 0.9 μ m, *Physical Review Letters* **81**, 4549 (1998).

[147] Z. Xu, P. Ju, X. Gao, K. Shen, Z. Jacob, and T. Li, Observation and control of Casimir effects in a sphere-plate-sphere system, *Nature Communications* **13**, 6148 (2022).

[148] P. Swinkels, S. Stuij, Z. Gong, H. Jonas, N. Ruffino, B. v. d. Linden, P. Bolhuis, S. Sacanna, S. Woutersen, and P. Schall, Revealing pseudorotation and ring-opening reactions in colloidal organic molecules, *Nature Communications* **12**, 2810 (2021).

[149] C. Bechinger, R. Di Leonardo, H. Löwen, C. Reichhardt, G. Volpe, and G. Volpe, Active particles in complex and crowded environments, *Reviews of Modern Physics* **88**, 045006 (2016).

[150] J. Elgeti, R. G. Winkler, and G. Gompper, Physics of microswimmers—single particle motion and collective behavior: a review, *Reports on Progress in Physics* **78**, 056601 (2015).

[151] E. Lauga, Bacterial hydrodynamics, *Annual Review of Fluid Mechanics* **48**, 105–130 (2016).

[152] M. Huang, W. Hu, S. Yang, Q.-X. Liu, and H. Zhang, Circular swimming motility and disordered hyperuniform state in an algae system, *Proceedings of the National Academy of Sciences* **118**, e2100493118 (2021).

[153] S. Kamdar, S. Shin, P. Leishangthem, L. F. Francis, X. Xu, and X. Cheng, The colloidal nature of complex fluids enhances bacterial motility, *Nature* **603**, 819–823 (2022).

[154] H. J. Jeong, S. Y. Lee, N. S. Kang, Y. D. Yoo, A. S. Lim, M. J. Lee, H. S. Kim, W. Yih, H. Yamashita, and T. C. LaJeunesse, Genetics and morphology characterize the dinoflagellate Symbiodinium voratum, n. sp.,(Dinophyceae) as the sole representative of Symbiodinium clade E, *Journal of Eukaryotic Microbiology* **61**, 75–94 (2014).

[155] R. F. Campos, H. Bachimanchi, G. Volpe, and K. Villa, Bubble-propelled micromotors for ammonia generation, *Nanoscale* **15**, 15785–15793 (2023).

[156] S. Das, M. Ciarchi, Z. Zhou, J. Yan, J. Zhang, and R. Alert, Flocking by turning away, *Physical Review X* **14**, 031008 (2024).

[157] I. Buttinoni, G. Volpe, F. Kümmel, G. Volpe, and C. Bechinger, Active Brownian motion tunable by light, *Journal of Physics: Condensed Matter* **24**, 284129 (2012).

[158] J. R. Howse, R. A. Jones, A. J. Ryan, T. Gough, R. Vafabakhsh, and R. Golestanian, Self-motile colloidal particles: from directed propulsion to random walk, *Physical Review Letters* **99**, 048102 (2007).

[159] H. Wang, G. Zhao, and M. Pumera, Beyond platinum: bubble-propelled micromotors based on Ag and MnO2 catalysts, *Journal of the American Chemical Society* **136**, 2719–2722 (2014).

[160] W. Gao, X. Feng, A. Pei, Y. Gu, J. Li, and J. Wang, Seawater-driven magnesium based Janus micromotors for environmental remediation, *Nanoscale* **5**, 4696–4700 (2013).

[161] L. Ren, W. Wang, and T. E. Mallouk, Two forces are better than one: combining chemical and acoustic propulsion for enhanced micromotor functionality, *Accounts of Chemical Research* **51**, 1948–1956 (2018).

[162] J. Palacci, S. Sacanna, A. P. Steinberg, D. J. Pine, and P. M. Chaikin, Living crystals of light-activated colloidal surfers, *Science* **339**, 936–940 (2013).

[163] B. Dai, J. Wang, Z. Xiong, X. Zhan, W. Dai, C.-C. Li, S.-P. Feng, and J. Tang, Programmable artificial phototactic microswimmer, *Nature Nanotechnology* **11**, 1087–1092 (2016).

[164] D. P. Singh, U. Choudhury, P. Fischer, and A. G. Mark, Non-equilibrium assembly of light-activated colloidal mixtures, *Advanced Materials* **29**, 1701328 (2017).

[165] Y. Alapan, U. Bozuyuk, P. Erkoc, A. C. Karacakol, and M. Sitti, Multifunctional surface microrollers for targeted cargo delivery in physiological blood flow, *Science Robotics* **5**, eaba5726 (2020).

[166] H. Xu, M. Medina-Sánchez, M. F. Maitz, C. Werner, and O. G. Schmidt, Sperm micromotors for cargo delivery through flowing blood, *ACS nano* **14**, 2982–2993 (2020).

[167] H. Xu, S. Wu, Y. Liu, X. Wang, A. K. Efremov, L. Wang, J. S. McCaskill, M. Medina-Sánchez, and O. G. Schmidt, 3D nanofabricated soft microrobots with super-compliant picoforce springs as onboard sensors and actuators, *Nature Nanotechnology* **19**, 494–503 (2024).

[168] J. Li, T. Li, T. Xu, M. Kiristi, W. Liu, Z. Wu, and J. Wang, Magneto–acoustic hybrid nanomotor, *Nano Letters* **15**, 4814–4821 (2015).

[169] X. Lu, K. Zhao, W. Liu, D. Yang, H. Shen, H. Peng, X. Guo, J. Li, and J. Wang, A human microrobot interface based on acoustic manipulation, *Acs Nano* **13**, 11443–11452 (2019).

[170] S. Palagi, A. G. Mark, S. Y. Reigh, K. Melde, T. Qiu, H. Zeng, C. Parmeggiani, D. Martella, A. Sanchez-Castillo, N. Kapernaum,*et al.*, Structured light enables biomimetic swimming and versatile locomotion of photoresponsive soft microrobots, *Nature Materials* **15**, 647–653 (2016).

[171] A. Aubret, Q. Martinet, and J. Palacci, Metamachines of pluripotent colloids, *Nature Communications* **12**, 6398 (2021).

[172] T. Bäuerle, A. Fischer, T. Speck, and C. Bechinger, Self-organization of active particles by quorum sensing rules, *Nature Communications* **9**, 3232 (2018).

[173] M. Sitti and D. S. Wiersma, Pros and cons: Magnetic versus optical microrobots, *Advanced Materials* **32**, 1906766 (2020).

[174] F. Rajabasadi, L. Schwarz, M. Medina-Sánchez, and O. G. Schmidt, 3D and 4D lithography of untethered microrobots, *Progress in Materials Science* **120**, 100808 (2021).

[175] G. T. Iványi, B. Nemes, I. Gróf, T. Fekete, J. Kubacková, Z. Tomori, G. Bánó, G. Vizsnyiczai, and L. Kelemen, Optically Actuated soft Microrobot Family for Single-cell Manipulation, *Advanced Materials* page 2401115 (2024).

[176] D. B. Phillips, G. M. Gibson, R. Bowman, M. J. Padgett, S. Hanna, D. M. Carberry, M. J. Miles, and S. H. Simpson, An optically actuated surface scanning probe, *Optics Express* **20**, 29679–29693 (2012).

[177] F. Schmidt, A. Magazzù, A. Callegari, L. Biancofiore, F. Cichos, and G. Volpe, Microscopic engine powered by critical demixing, *Physical Review Letters* **120**, 068004 (2018).

[178] H. Zeng, P. Wasylczyk, C. Parmeggiani, D. Martella, M. Burresi, and D. S. Wiersma, Light-fueled microscopic walkers, *Advanced Materials (Deerfield Beach, Fla.)* **27**, 3883 (2015).

[179] Y. Y. Tanaka, P. Albella, M. Rahmani, V. Giannini, S. A. Maier, and T. Shimura, Plasmonic linear nanomotor using lateral optical forces, *Science Advances* **6**, eabc3726 (2020).

[180] X. Wu, R. Ehehalt, G. Razinskas, T. Feichtner, J. Qin, and B. Hecht, Light-driven microdrones, *Nature Nanotechnology* **17**, 477–484 (2022).

[181] M. E. Friese, T. A. Nieminen, N. R. Heckenberg, and H. Rubinsztein-Dunlop, Optical alignment and spinning of laser-trapped microscopic particles, *Nature* **394**, 348–350 (1998).

[182] M. Friese, H. Rubinsztein-Dunlop, J. Gold, P. Hagberg, and D. Hanstorp, Optically driven micromachine elements, *Applied Physics Letters* **78**, 547–549 (2001).

[183] S. L. Neale, M. P. MacDonald, K. Dholakia, and T. F. Krauss, All-optical control of microfluidic components using form birefringence, *Nature Materials* **4**, 530–533 (2005).

[184] H. He, M. Friese, N. Heckenberg, and H. Rubinsztein-Dunlop, Direct observation of transfer of angular momentum to absorptive particles from a laser beam with a phase singularity, *Physical Review Letters* **75**, 826 (1995).

[185] Z. Yan and N. F. Scherer, Optical vortex induced rotation of silver nanowires, *The Journal of Physical Chemistry Letters* **4**, 2937–2942 (2013).

[186] A. Lehmuskero, Y. Li, P. Johansson, and M. Käll, Plasmonic particles set into fast orbital motion by an optical vortex beam, *Optics Express* **22**, 4349–4356 (2014).

[187] X. Chen, Y. Chen, M. Yan, and M. Qiu, Nanosecond photothermal effects in plasmonic nanostructures, *ACS Nano* **6**, 2550–2557 (2012).

[188] J.-S. Huang, V. Callegari, P. Geisler, C. Brüning, J. Kern, J. C. Prangsma, X. Wu, T. Feichtner, J. Ziegler, P. Weinmann,*et al.*, Atomically flat single-crystalline gold nanostructures for plasmonic nanocircuitry, *Nature Communications* **1**, 150 (2010).

[189] C. A. Mack, Fifty years of Moore's law, *IEEE Transactions on semiconductor manufacturing* **24**, 202–207 (2011).

[190] M. Fernández-Medina, M. A. Ramos-Docampo, O. Hovorka, V. Salgueiriño, and B. Städler, Recent advances in nano-and micromotors, *Advanced Functional Materials* **30**, 1908283 (2020).

[191] Y.-C. Tai and R. S. Muller, IC-processed electrostatic synchronous micromotors, *Sensors and Actuators* **20**, 49–55 (1989).

[192] O. Solgaard, A. A. Godil, R. T. Howe, L. P. Lee, Y.-A. Peter, and H. Zappe, Optical MEMS: From micromirrors to complex systems, *Journal of Microelectromechanical systems* **23**, 517–538 (2014).

[193] M. C. Wu, Micromachining for optical and optoelectronic systems, *Proceedings of the IEEE* **85**, 1833–1856 (1997).

[194] J. W. Judy, Microelectromechanical systems (MEMS): fabrication, design and applications, *Smart materials and Structures* **10**, 1115 (2001).

[195] S. Maruo and H. Inoue, Optically driven micropump produced by three-dimensional two-photon microfabrication, *Applied Physics Letters* **89** (2006).

[196] L.-S. Fan, Y.-C. Tai, and R. S. Muller, IC-processed electrostatic micromotors, *Sensors and Actuators* **20**, 41–47 (1989).

[197] A. Fennimore, T. Yuzvinsky, W.-Q. Han, M. Fuhrer, J. Cumings, and A. Zettl, Rotational actuators based on carbon nanotubes, *Nature* **424**, 408–410 (2003).

[198] N. Ghalichechian, A. Modafe, M. I. Beyaz, and R. Ghodssi, Design, fabrication, and characterization of a rotary micromotor supported on microball bearings, *Journal of Microelectromechanical Systems* **17**, 632–642 (2008).

[199] H. Xia, J. Wang, Y. Tian, Q.-D. Chen, X.-B. Du, Y.-L. Zhang, Y. He, and H.-B. Sun, Ferrofluids for fabrication of remotely controllable micro-nanomachines by two-photon polymerization, *Advanced Materials* **22**, 3204–3207 (2010).

[200] T. Zandrini, S. Taniguchi, and S. Maruo, Magnetically driven micromachines created by two-photon microfabrication and selective electroless magnetite plating for lab-on-a-chip applications, *Micromachines* **8**, 35 (2017).

[201] W. Wang, J. Giltinan, S. Zakharchenko, and M. Sitti, Dynamic and programmable self-assembly of micro-rafts at the air-water interface, *Science Advances* **3**, e1602522 (2017).

[202] H. Wang, B.-B. Xu, Y.-L. Zhang, P. S. Kollipara, S. Liu, L. Lin, Q.-D. Chen, Y. Zheng, and H.-B. Sun, Light-driven magnetic encoding for hybrid magnetic micromachines, *Nano Letters* **21**, 1628–1635 (2021).

[203] Z. Liu, M. Li, X. Dong, Z. Ren, W. Hu, and M. Sitti, Creating three-dimensional magnetic functional microdevices via molding-integrated direct laser writing, *Nature Communications* **13**, 2016 (2022).

[204] C. W. Shields IV, K. Han, F. Ma, T. Miloh, G. Yossifon, and O. D. Velev, Supercolloidal spinners: Complex active particles for electrically powered and switchable rotation, *Advanced Functional Materials* **28**, 1803465 (2018).

[205] X. Hong, B. Xu, G. Li, F. Nan, X. Wang, Q. Liang, W. Dong, W. Dong, H. Sun, Y. Zhang,*et al.*, Optoelectronically navigated nano-kirigami microrotors, *Science Advances* **10**, eadn7582 (2024).

[206] X. Shi, A.-K. Pumm, C. Maffeo, F. Kohler, E. Feigl, W. Zhao, D. Verschueren, R. Golestanian, A. Aksimentiev, H. Dietz,*et al.*, A DNA turbine powered by a transmembrane potential across a nanopore, *Nature Nanotechnology* **19**, 338–344 (2024).

[207] L. Kelemen, S. Valkai, and P. Ormos, Integrated optical motor, *Applied Optics* **45**, 2777–2780 (2006).

[208] S. Bianchi, G. Vizsnyiczai, S. Ferretti, C. Maggi, and R. Di Leonardo, An optical reaction micro-turbine, *Nature Communications* **9**, 4476 (2018).

[209] S. P. Radzevich and D. W. Dudley, *Handbook of Practical Gear Design*, CRC press (1994).

[210] E. J. Garcia and J. J. Sniegowski, Surface micromachined microengine, *Sensors and Actuators A: Physical* **48**, 203–214 (1995).

[211] P. Galajda and P. Ormos, Complex micromachines produced and driven by light, In *Summaries of Papers Presented at the Lasers and Electro-Optics. CLEO'02. Technical Diges*, pages 634–635, IEEE (2002).

[212] J. Sniegowski and E. Garcia, Surface-micromachined gear trains driven by an on-chip electrostatic microengine, *IEEE Electron Device Letters* **17**, 366–368 (1996).

[213] C. Liu, J. Zhao, F. Tian, L. Cai, W. Zhang, Q. Feng, J. Chang, F. Wan, Y. Yang, B. Dai,*et al.*, Low-cost thermophoretic profiling of extracellular-vesicle surface proteins for the early detection and classification of cancers, *Nature Biomedical Engineering* **3**, 183–193 (2019).

[214] B. Ciraulo, J. Garcia-Guirado, I. de Miguel, J. Ortega Arroyo, and R. Quidant, Long-range optofluidic control with plasmon heating, *Nature Communications* **12**, 2001 (2021).

[215] A. Terray, J. Oakey, and D. W. Marr, Microfluidic control using colloidal devices, *Science* **296**, 1841–1844 (2002).

[216] S. H. Lee, D. Van Noort, J. Y. Lee, B.-T. Zhang, and T. H. Park, Effective mixing in a microfluidic chip using magnetic particles, *Lab on a Chip* **9**, 479–482 (2009).

[217] D. Psaltis, S. R. Quake, and C. Yang, Developing optofluidic technology through the fusion of microfluidics and optics, *Nature* **442**, 381–386 (2006).

[218] X. Fan and I. M. White, Optofluidic microsystems for chemical and biological analysis, *Nature Photonics* **5**, 591–597 (2011).

[219] D. R. Link, E. Grasland-Mongrain, A. Duri, F. Sarrazin, Z. Cheng, G. Cristobal, M. Marquez, and D. A. Weitz, Electric control of droplets in microfluidic devices, *Angewandte Chemie International Edition* **45**, 2556 (2006).

[220] M. Stepanova and S. Dew, *Nanofabrication: techniques and principles*, Springer Science & Business Media (2011).

[221] M. J. Madou, *Fundamentals of microfabrication: the science of miniaturization*, CRC press (2018).

[222] M. Tröndle, O. Zvyagolskaya, A. Gambassi, D. Vogt, L. Harnau, C. Bechinger, and S. Dietrich, Trapping colloids near chemical stripes via critical Casimir forces, *Molecular Physics* **109**, 1169–1185 (2011).

[223] S. Kondrat, L. Harnau, and S. Dietrich, Critical Casimir interaction of ellipsoidal colloids with a planar wall, *The Journal of Chemical Physics* **131** (2009).

[224] O. Vasilyev, E. Eisenriegler, and S. Dietrich, Critical Casimir torques and forces acting on needles in two spatial dimensions, *Physical Review E—Statistical, Nonlinear, and Soft Matter Physics* **88**, 012137 (2013).

[225] N. Farahmand Bafi, P. Nowakowski, and S. Dietrich, Effective pair interaction of patchy particles in critical fluids, *The Journal of Chemical Physics* **152** (2020).

[226] G. Wang, P. Nowakowski, N. Farahmand Bafi, B. Midtvedt, F. Schmidt, A. Callegari, R. Verre, M. Käll, S. Dietrich, S. Kondrat,*et al.*, Nanoalignment by critical Casimir torques, *Nature Communications* **15**, 5086 (2024).

[227] L. Soler, V. Magdanz, V. M. Fomin, S. Sanchez, and O. G. Schmidt, Self-propelled micromotors for cleaning polluted water, *ACS Nano* **7**, 9611–9620 (2013).

[228] M. Urso, M. Ussia, and M. Pumera, Smart micro-and nanorobots for water purification, *Nature Reviews Bioengineering* **1**, 236–251 (2023).

[229] L. Korson, W. Drost-Hansen, and F. J. Millero, Viscosity of water at various temperatures, *The Journal of Physical Chemistry* **73**, 34–39 (1969).

[230] K. Ladavac and D. G. Grier, Microoptomechanical pumps assembled and driven by holographic optical vortex arrays, *Optics Express* **12**, 1144–1149 (2004).

[231] P. Nowakowski, N. F. Bafi, G. Volpe, S. Kondrat, and S. Dietrich, Critical Casimir levitation of colloids above a bull's-eye pattern, *arXiv preprint arXiv:2409.08366* (2024).

[232] J. C. Ndukaife, A. V. Kildishev, A. G. A. Nnanna, V. M. Shalaev, S. T. Wereley, and A. Boltasseva, Long-range and rapid transport of individual nano-objects by a hybrid electrothermoplasmonic nanotweezer, *Nature Nanotechnology* **11**, 53–59 (2016).

[233] M. A. Fernandez-Rodriguez, F. Grillo, L. Alvarez, M. Rathlef, I. Buttinoni, G. Volpe, and L. Isa, Feedback-controlled active brownian colloids with space-dependent rotational dynamics, *Nature Communications* **11**, 4223 (2020).

[234] G. Muñoz-Gil, G. Volpe, M. A. Garcia-March, E. Aghion, A. Argun, C. B. Hong, T. Bland, S. Bo, J. A. Conejero, N. Firbas,*et al.*, Objective comparison of methods to decode anomalous diffusion, *Nature Communications* **12**, 6253 (2021).

[235] X. Cao, E. Panizon, A. Vanossi, N. Manini, and C. Bechinger, Orientational and directional locking of colloidal clusters driven across periodic surfaces, *Nature Physics* **15**, 776–780 (2019).

[236] X. Cao, A. Silva, E. Panizon, A. Vanossi, N. Manini, E. Tosatti, and C. Bechinger, Moiré-pattern evolution couples rotational and translational friction at crystalline interfaces, *Physical Review X* **12**, 021059 (2022).

[237] J. Liu, D. Wu, and S. Zeng, Influence of temperature and layers on the characterization of ITO films, *Journal of Materials Processing Technology* **209**, 3943–3948 (2009).

[238] M. Virk, K. Xiong, M. Svedendahl, M. Kall, and A. B. Dahlin, A thermal plasmonic sensor platform: resistive heating of nanohole arrays, *Nano Letters* **14**, 3544–3549 (2014).

[239] A. R. Anwar, M. T. Sajjad, M. A. Johar, C. A. Hernández-Gutiérrez, M. Usman, and S. Łepkowski, Recent progress in micro-LED-based display technologies, *Laser & Photonics Reviews* **16**, 2100427 (2022).

[240] X. Zhou, P. Tian, C.-W. Sher, J. Wu, H. Liu, R. Liu, and H.-C. Kuo, Growth, transfer printing and colour conversion techniques towards full-colour micro-LED display, *Progress in Quantum Electronics* **71**, 100263 (2020).

[241] B. Munkhbat, A. Canales, B. Küçüköz, D. G. Baranov, and T. O. Shegai, Tunable self-assembled Casimir microcavities and polaritons, *Nature* **597**, 214–219 (2021).

[242] T.-Y. Huang, H. Gu, and B. J. Nelson, Increasingly intelligent micromachines, *Annual Review of Control, Robotics, and Autonomous Systems* **5**, 279–310 (2022).

[243] A. C. Tsang, E. Demir, Y. Ding, and O. S. Pak, Roads to smart artificial microswimmers, *Advanced Intelligent Systems* **2**, 1900137 (2020).

[244] S. Lu, L. Hou, and F. Gan, Preparation and optical properties of phase-change VO2 thin films, *Journal of Materials Science* **28**, 2169–2177 (1993).

[245] G. Kocak, C. Tuncer, and V. Bütün, pH-Responsive polymers, *Polymer Chemistry* **8**, 144–176 (2017).

[246] D. Schmaljohann, Thermo-and pH-responsive polymers in drug delivery, *Advanced Drug Delivery Reviews* **58**, 1655–1670 (2006).

[247] H. Zeng, P. Wasylczyk, D. S. Wiersma, and A. Priimagi, Light robots: bridging the gap between microrobotics and photomechanics in soft materials, *Advanced Materials* **30**, 1703554 (2018).

[248] Q. Liu, W. Wang, M. F. Reynolds, M. C. Cao, M. Z. Miskin, T. A. Arias, D. A. Muller, P. L. McEuen, and I. Cohen, Micrometer-sized electrically programmable shape-memory actuators for low-power microrobotics, *Science Robotics* **6**, eabe6663 (2021).

[249] K. Bertoldi, V. Vitelli, J. Christensen, and M. Van Hecke, Flexible mechanical metamaterials, *Nature Reviews Materials* **2**, 1–11 (2017).

[250] P. Baconnier, D. Shohat, C. H. López, C. Coulais, V. Démery, G. Düring, and O. Dauchot, Selective and collective actuation in active solids, *Nature Physics* **18**, 1234–1239 (2022).

[251] I. Grexa, T. Fekete, J. Molnár, K. Molnár, G. Vizsnyiczai, P. Ormos, and L. Kelemen, Single-cell elasticity measurement with an optically actuated microrobot, *Micromachines* **11**, 882 (2020).

[252] M. M. de Souza Lima and R. Borsali, Rodlike cellulose microcrystals: structure, properties, and applications, *Macromolecular Rapid Communications* **25**, 771–787 (2004).